Rivista Italiana di Paleontologia e Stratigrafia
(*Research in Paleontology and Stratigraphy*)
vol. 131(3): 687-721. **November 2025**
DOI: https://doi.org/10.54103/2039-4942/26086

A NEW SPECIMEN OF *MACROPLACUS RAETICUS* SCHUBERT-KLEMPNAUER, 1975 (SAUROPTERYGIA, PLACODONTIA) FROM THE UPPER TRIASSIC OF ITALY, WITH REMARKS ON PLACODONT PHYLOGENY

STEFANIA NOSOTTI[1*], FEDERICO CONFORTINI[2] & SIMONE MAGANUCO[3]

[1]Museo di Storia Naturale di Milano, Milano, Italy. E-mail: stefanianosotti@yahoo.it
[2]Museo Civico di Scienze Naturali "Enrico Caffi" di Bergamo, Bergamo, Italy. E-mail: federico.confortini@comune.bergamo.it
[3]Museo di Storia Naturale di Milano, Milano, Italy. E-mail: simonemaganuco@iol.it
*Corresponding author.

Associate Editor: Silvio Renesto.

To cite this article: Nosotti S., Confortini F. & Maganuco S. (2025) - A new specimen of *Macroplacus raeticus* Schubert-Klempnauer, 1975 (Sauropterygia, Placodontia) from the Upper Triassic of Italy, with remarks on placodont phylogeny. *Rivista Italiana di Paleontologia e Stratigrafia*, vol. 131(3): 687-721.

Keywords: Zu Limestone; Orobic Alps; Cyamodontoidea; skull; dentition; character description and coding.

Abstract. A new placodont specimen—an incomplete, three-dimensionally preserved skull encased in a carbonate matrix—is described here. Although discovered in slope debris, strong evidence suggests that the fossil most likely originated from the Rhaetian (Upper Triassic) Zu Limestone. Anatomical study—including X-ray computed tomography (CT)—comparison with other placodont species, and phylogenetic analysis support attribution of the new specimen to the cyamodontoid placodont *Macroplacus raeticus* Schubert-Klempnauer, 1975. Until now, this species was known solely from its holotype: a skull from the Rhaetian of the Bavarian Alps, which we have re-examined and, in part, reinterpreted. The new specimen shows the closest morphological affinity to the *Macroplacus* holotype among all known placodonts; the significant size difference between the two is explained as representing different ontogenetic stages of the same taxon. Our species-level phylogenetic analysis of Placodontia supports a sister-taxon relationship between the new specimen and *Macroplacus*. The analysis builds upon previous studies, incorporating revised descriptions and updated character coding for a substantial number of skull traits, the addition of new characters and taxa, and overall improvements to the phylogenetic dataset for current and future analyses. *Macroplacus raeticus* remains the only placodont species known exclusively from the Rhaetian. Along with the morphologically similar *Psephoderma alpinum*—from the Norian and Rhaetian—it represents the latest occurrence of placodonts in the Upper Triassic, strengthening the case for a close evolutionary relationship between these two taxa.

Received: September 15, 2024; accepted: August 4, 2025

Introduction

Placodontia represents the basalmost group within Sauropterygia (e.g. Wang et al. 2019b), a lineage of aquatic reptiles that became one of the most successful in Earth's history. Sauropterygians radiated into Mesozoic seas and oceans from the latest Early Triassic to the very end of the Late Cretaceous, including pelagic taxa such as plesiosaurs and pliosaurs—some of the most iconic prehistoric animals in the collective imagination (Motani 2009; Neenan et al. 2013; Rieppel 1997 and 2000a).

Placodonts inhabited intraplatform basins and epicontinental seas of the eastern and western Tethyan Realms, where they evolved remarkable specialisations for durophagy, feeding on hard-shelled prey (Gere et al. 2024; Neenan et al. 2013; Rieppel 2001a and 2002a). The most derived members of the clade, the Cyamodontoidea, were heavily armoured with turtle-like carapaces (Rieppel 2002b) and exhibited extreme adaptations for durophagy. These include significant cranial modifications, with the development of a largely ossified braincase and the loss of cranial kinesis (Nosotti & Pinna 1996; Rieppel 2001b). Additionally, as noted by Gere et al. (2024), the more specialised placodonts show a progressive reduction in tooth number, an increase in the size of posterior palatine tooth-plates, an elongation of the premaxillary rostrum, and a widening of the temporal region, all of which are presumably linked to dietary adaptations.

Placodont fossils were first discovered and described from the lower Middle Triassic (Anisian) to the uppermost Upper Triassic (Rhaetian), with remains reported from Europe, North Africa, and the Middle East (Nosotti & Pinna 1989 and references therein; Rieppel 1999; Rieppel et al. 1999 and references therein). These localities correspond to nearshore environments along the western margin of the Tethys Ocean.

However, the discovery of the cyamodontoid placodont *Sinocyamodus xinpuensis* (Li 2000) from the Carnian upper Falang Formation (Wayao Member) of Guizhou Province, southwestern China, revealed that placodonts also inhabited the eastern Tethyan margin, corresponding to the geographic range of the present-day southwestern China. Since then, additional Chinese placodont species have been described, representing both unarmoured or partially armoured, plesiomorphic Placodontoidea—such as *Placodus inexpectatus* (Jiang et al. 2008; Neenan et al. 2015) from the Anisian upper Guanling Formation of Guizhou Province (Xing et al. 2020)—and derived, armoured Cyamodontoidea. Among the Cyamodontoidea are the above-mentioned *Sinocyamodus xinpuensis* (Li 2000; Neenan et al. 2015; Wang et al. 2019c), as well as the coeval *Cyamodus orientalis* (Wang et al. 2019a) and *Psephochelys polyosteoderma* (Li & Rieppel 2002; Neenan et al. 2015; Wang et al. 2019b). All these are from the upper Falang Formation of Guizhou Province (Wayao Member, Carnian) (Wang et al. 2010; Zou et al. 2015). Additionally, two species of the placochelyid *Glyphoderma* were described from the lower Falang Formation (Zhuganpo Member, Ladinian) of Yunnan Province (Wang et al. 2010; Zou et al. 2015; Neenan et al. 2015): *Glyphoderma kangi* (Zhao et al. 2008) and *Glyphoderma robusta* (Hu et al. 2019).

This growing body of evidence has significantly advanced our understanding of placodont interrelationships, evolutionary history, and biogeographic origins. Recent cladistic analyses have expanded on previous studies (Rieppel 2000b, 2001b; Jiang et al. 2008; see "Placodont phylogenetic analysis" and "Supplementary contents") by incorporating newly described cranial and postcranial characters from exceptionally well-preserved Chinese specimens (Neenan et al. 2015; Wang et al. 2019b and references therein) as well as from newly discovered western European specimens (de Miguel Chaves et al. 2018b and 2020). These analyses show that placodonts from the eastern Tethyan Realm are interspersed among European taxa throughout the cladograms, indicating that Chinese placodonts do not form a monophyletic group and suggesting extensive interchange between eastern and western Tethyan populations during the Middle and Late Triassic, with no major geographic separation (Neenan et al. 2015; Wang et al. 2019a). Similar biogeographic patterns are observed in other sauropterygian groups that occur in both Central Europe and southwest China (Wang et al. 2019a and references therein). Additionally, current phylogenetic studies confirm that Placodontia is monophyletic, with basal Placodontoidea forming the sister group to a monophyletic Cyamodontoidea, which encompasses both the fully armoured Cyamodontida and Placochelyida.

Within Cyamodontida, *Cyamodus orientalis* extends the geographic range of the genus *Cyamodus* to the eastern Tethyan Province, confirming its occurrence in the Upper Triassic (early Carnian) (Wang et al. 2019a), as previously suggested by Rieppel & Nosotti (2001) and Buffetaut & Novak (2008) based on skull remains from Europe (contra Wang et al. 2019a: p.18).

Within Placochelyida, a revised Placochelyidae, incorporating Chinese taxa, has been identified (Neenan et al. 2015). This clade represents the most derived placodont bauplan from the Upper Triassic. The discovery of *Glyphoderma* from the Ladinian, extends the stratigraphic range of placochelyids into the Middle Triassic, whereas they were previously known only from the Upper Triassic of Europe. According to Neenan et al. (2015), this supports an eastern origin of Placochelyidae, although future discoveries may challenge this interpretation. Notably, Upper Triassic European placochelyids were the longest-surviving placodonts, with *Psephoderma* persisting until the Rhaetian (latest Triassic), and *Macroplacus* known exclusively from the Rhaetian (Neenan et al. 2015). Within this context, *Macroplacus* remains of particular interest, as several morphological features of its holotype—the only known specimen until now—remain debated (see below). As a result, its phylogenetic position is still uncertain, despite exhibiting dental morphology, tooth formula, and replacement patterns similar to those of Placochelyidae (Rieppel 2001a; Neenan et al. 2014).

In this paper we describe a new placodont specimen housed in the Palaeontological Collections of the Museo Civico di Scienze Naturali "E. Caffi" (Bergamo, Italy). This specimen represents the second known occurrence of *Macroplacus raeticus* worldwide and the first from Italy (Bergamo Province, northern Italy). It originates from the Zu Limestone (Rhaetian) and consists of an incomplete, three-dimensionally preserved skull enclosed in limestone matrix, featuring large, sub-round tooth-plates. We test its attribution to *Macroplacus raeticus* through anatomical description, X-ray computed tomography (CT) data, morphological comparisons, and phylogenetic analysis.

Additionally, we reassess the cranial morphology of *Macroplacus raeticus* holotype, propose an amended diagnosis of the monotypic genus, and discuss the monophyly and interrelationships of Placochelyidae (sensu Neenan et al. 2015).

Institutional abbreviations

FAFI = Magyar Állami Földtani Intézet, Budapest, Hungary.

MB.R. = Museum für Naturkunde der Humboldt Universität, Berlin, Germany.

MCSNB = Museo Civico di Scienze Naturali "Enrico Caffi", Bergamo, Italy.

MHI = Muschelkalk Museum Hagdorn, Ingelfingen, Germany.

MFSN = Museo Friulano di Storia Naturale, Udine, Italy.

MSNM = Museo di Storia Naturale, Milano, Italy.

PIMUZ = Universität Zürich, Paläontologisches Institut, Switzerland.

SMF = Senckenberg Museum, Frankfurt a.M, Germany.

SMNS = Staatliches Museum für Naturkunde, Stuttgart, Germany.

SNSB-BSPG = Staatliche Naturwissenschaftliche Sammlungen Bayerns, Bayerische Staatssammlung für Paläontologie und Geologie, München, Germany.

UMO = Urwelt-Museum Oberfranken, Bayreuth, Germany.

The acronym "ST," as specified below, refers to the ongoing inventory conducted by the Italian State, which, according to current laws, owns all fossil specimens found within the national territory. Their conservation and study are managed by the "Soprintendenza ABAP (Archeologia, Belle Arti e Paesaggio)". The acronym "ST" itself does not indicate a specific conservation repository, as such decisions are made by the Soprintendenza, which carries out its institutional duties across different jurisdictional territories.

ST = Italian State inventory, managed by the Soprintendenza ABAP, Ministero della Cultura, Italy.

Materials and Methods

The specimen MCSNB 13033 described here, was discovered in 2010 by Mr. Pio Carlo Brizzi in Oschiolo locality (coordinates: 45°48'25.2"N 9°49'11.4"E), upstream from Orezzo village in Gazzaniga Municipality (Bergamo Province, Lombardy, northern Italy) (Fig. 1). It consists of an isolated, incomplete, three-dimensional skull enclosed in a limestone matrix (Figs. 2-4), preserving large, sub-round tooth-plates, which immediately suggested its affinity with placodonts.

The fossil was delivered in the same condition in which it was found to the Museo Civico di Scienze Naturali "Enrico Caffi" (Bergamo, Italy). Following the fortuitous discovery, the Soprintendenza ABAP was informed, and the specimen is now housed in the Palaeontological Collections of the Museo Civico di Scienze Naturali "Enrico Caffi", where it has been assigned the index number MCSNB 13033.

The discovery site is a non-anthropised, naturally wooded area at an elevation of approximately 750 m above sea level, near the eastern ridge of Monte Cedrina, and a few dozen meters upstream from CAI trail no. 524. Although the specimen was

found in slope debris, isolated from its original rocky substrate, the survey of the discovery site (discussed below) and the position strongly indicate that the fossil most likely originated from the Rhaetian Zu Limestone.

The following placodont skull specimens were personally (SN) examined for comparison:

SNSB-BSPG 1967 I 324 (formerly BSP 1967 I 324): holotype of *Macroplacus raeticus*, isolated, three-dimensionally preserved skull; Staatliche Naturwissenschaftliche Sammlungen Bayerns, Bayerische Staatssammlung für Paläontologie und Geologie, München, Germany.

MSNM V 471: *Psephoderma alpinum*, isolated, three-dimensionally preserved skull; Museo di Storia Naturale, Milano, Italy.

MCSNB 4614: *Psephoderma alpinum*, isolated skull fragments and lower jaws embedded in matrix; Museo Civico di Scienze Naturali "Enrico Caffi", Bergamo, Italy.

MFSN 1819 GP and 1923 GP: *Protenodontosaurus italicus*, isolated, three-dimensionally preserved skulls; Museo Friulano di Storia Naturale, Udine, Italy.

MFSN 26830: *Cyamodus* sp., isolated skull enclosed in matrix slab; Museo Friulano di Storia Naturale, Udine, Italy.

MSNM V 478: *Cyamodus hildegardis*, isolated skull enclosed in matrix slab; Museo di Storia Naturale, Milano, Italy.

SMNS 15855 and SMNS 16270: *Cyamodus kuhnschnyderi*, isolated, three-dimensionally preserved skulls; Staatliches Museum für Naturkunde, Stuttgart, Germany.

SMNS 17403: *Cyamodus rostratus*, isolated three-dimensionally preserved skull; Staatliches Museum für Naturkunde, Stuttgart, Germany.

SMF R 4038: *Placodus gigas*, skull fragment with a partial natural endocast of the braincase; Senckenberg Museum, Frankfurt a.M., Germany.

SMF R 359: *Placodus gigas*, skull with the supraoccipital and the parietal removed; Senckenberg Museum, Frankfurt a.M., Germany.

UMO BT13: *Placodus gigas*, isolated, three-dimensionally preserved skull; Urwelt-Museum Oberfranken, Bayreuth, Germany.

The MCSNB 13033 specimen underwent X-ray computed tomography (CT) at the Servizio di Radiologia, Ospedale Maggiore di Milano, using a Siemens Somatom Definition Dual Source CT Scanner. CT imaging was performed with bone and mediastinum algorithms on transverse (axial) slices, using the following parameters: 140 kV, 204 mA, 0.4 mm slice thickness. The scan data were exported in DICOM format via eFilm (v. 1.5.3, Merge eFilm, Toronto), and the 3D model was generated using the SYNGO.via Frontier System (Siemens). Image analyses and post-processing were carried out by Ilaria Paola Crippa (Siemens Milano), Giovanni Longhi (Siemens Milano), Manuel Cecchini (Siemens Milano) and Giovanni Terribile (TSRM dell'Ospedale Maggiore di Milano).

Despite its importance, the CT data did not yield well-defined images of the specimen's thin skull bones, as bone and matrix had similar radiodensity, making them difficult to distinguish. This limitation affected the 3D reconstruction, resulting in some artefacts (Fig. 4A-C). For instance, the palatine bones—clearly visible as a continuous thin layer in CT slices—appear absent in the 3D model, thereby exposing the underlying tooth-plate replacement cavities. Accordingly, CT-based interpretations were cross-checked directly against the original CT slice data (Fig. 4D-M). Despite these challenges, CT data proved crucial for identifying internal structures and sutures of the skull not visible externally (e.g., hard palate, braincase, dentition).

The three anatomical planes (Fig. 5) used to describe the CT slices are "midsagittal plane" (blue), "horizontal plane" (red), and "transverse (axial) plane" (purple), *sensu* Dahdul et al. (2014). We avoid using the term "coronal", which is frequently applied in human radiology but can cause confusion when describing most other vertebrates (Witmer, pers. comm., 2021). Therefore, our transverse (axial) plane corresponds to the coronal plane sensu Neenan et al. (2014).

When referring to the dental formula and tooth replacement stages, we follow the nomenclature of Neenan et al. (2014; see fig. 1 in that paper). Each tooth is designated as follows: right or left side of the skull (R or L), followed by the tooth-bearing element (pm, premaxilla; m, maxilla; pl, palatine; d, dentary), and then by the tooth position number, where 1 represents the most anterior (palatal dentition) or mesial (marginal dentition). Regarding the replacement stages of the tooth-plates, Neenan et al. (2014, p. 3) describe three stages, "based mostly on the state of growth of the enamel cap".

Unless otherwise specified, the nomenclature of taxa follows the results of the phylogenetic analysis presented in this paper, which is originally based on Wang et al. (2019a) and reprocessed datasets from previous studies (see "Placodont phylogenetic analysis" and Fig. 9). We retained all placodont species from prior analyses and included the recently described *Parahenodus atancensis* (de Miguel Chaves et al. 2018b). Here and in all previous studies, *Palatodonta bleekeri* (Neenan et al. 2013) consistently emerges as the sister group to Placodontia, with the latter encompassing all other placodont species within the Placodontiformes, excluding *Palatodonta*. Furthermore, there is broad consensus that Placodontoidea and Cyamodontoidea are sister groups, each containing essentially the same taxa. However, the specific sister group relationships within these clades, defined by a given set of synapomorphies, vary among different authors and will be discussed throughout this paper.

For clarity, when describing or discussing anatomical characters, we refer to their assigned number in the character list. Some characters cannot be determined in MCSNB 13033 due to incomplete preservation—this applies particularly to characters 2, 4-6, 11, 17, 21-33, 45-57, 59, 62-64, 67-88, and 90. Postcranial characters 63 and 68-88 are uncodable for MCSNB 13033 and for the holotype of *Macroplacus*, as both specimens are isolated skulls with no associated postcranial remains.

Anatomical abbreviations

acpn accessory connection palate-neurocranium; **an** apertura nasi ossea; **as** alveolar space; **bo** basioccipital; **bs** basisphenoid; **ccf** cerebral carotid foramen; **dlf** dental lamina foramen; **ept** epipterygoid; **eo** exoccipital; **f** frontal; **j** jugal; **laf** lacrimal foramen; **if** infraorbital foramen; **lf** labial foramen for cutaneous branch of superior alveolar nerve; **in** internal nares; **Lmx1** left anterior maxillary tooth-plate; **Lmx2** left posterior maxillary tooth-plate; **Lpl1** left anterior palatine tooth-plate; **Lpl2** left posterior palatine tooth-plate; **m** maxilla; **n** nasal; **o** orbit; **oc** otic capsule; **odp** opisthotic descending process; **osp** otic squamosal process; **p** parietal; **pbs** parabasisphenoid complex; **pcr** palatoquadrate cartilage recess; **pf** pineal foramen; **pl** palatine; **pm** premaxilla; **po** postorbital; **pof** postfrontal; **pop** paroccipital process of the opisthotic; **potF** post-temporal fenestra; **pr** prootic; **prf** prefrontal; **prF** prootic fenestra; **pt** pterygoid; **ptap** pterygoid ascending process; **ptf** pterygoid flange; **ptof** pteroccipital foramen; **pvf** parietal ventral flange; **q** quadrate; **qf** quadrate foramen; **qj** quadratojugal; **r.Lpl1** replacement left anterior palatine tooth-plate; **r.Rpl2** replacement right posterior palatine tooth-plate; **Rmx1** right anterior maxillary tooth-plate; **Rmx2** right posterior maxillary tooth-plate; **Rpl1** right anterior palatine tooth-plate; **Rpl2** right posterior palatine tooth-plate; **so** supraoccipital; **sq** squamosal; **sqb** squamosal buttress; **st** sella turcica; **stF** subtemporal fossa; **utF** upper temporal fenestra.

Geological setting

During the Early Triassic, a marine transgression was responsible for the deposition of mixed siliciclastic and carbonate deposits in the Lombardy Basin (Southern Alps). With the Middle Triassic, carbonate production increased, marked during the Ladinian by the development of high-relief carbonate platforms characterised by prograding slopes towards intraplatform basins.

Close to the Ladinian–Carnian boundary, a major sea-level fall exposed the top of the carbonate platforms of the Lombardy Basin. A renewed phase of carbonate production characterises the lower Carnian (Breno Formation) in the north, whereas alluvial/deltaic deposits (Val Sabbia Sandstone) passing to lagoonal facies (Gorno Formation) were deposited in the south. After the deposition of the sabkha facies of the San Giovanni Bianco Formation, a huge carbonate platform (Dolomia Principale Formation) developed. The Dolomia Principale Formation was affected by syndepositional extensional tectonics (Jadoul et al. 1994) that led to the development of intraplatform basins (Dolomie Zonate Formation and Zorzino Limestone). The Dolomia Principale Formation ends with a subaerial exposure (Berra et al. 2010) predating the abrupt clay input close to the Norian–Rhaetian boundary that characterises the Riva di Solto Shale and Zu Limestone. These formations were deposited first in the previously developed Norian intraplatform basins (covering the Zorzino Limestone) and only later covered the Dolomia Principale Formation highs. The abrupt input of clay in the Rhaetian documents an important climate change (Berra 2012) marking the demise of the Dolomia Principale system followed by a gradual recovery of carbonate production from the Riva di Solto Shale to the Zu Limestone, characterised in its upper part by the development of coral rich intervals. A gradual decrease of the water depth as well as a decrease of the abundance of clay and an increase of carbonate production is also recorded in the Rhaetian succession of the Lombardy Basin, with the development of depositional conditions interpreted as a ramp setting (Jadoul et al. 1994).

After the Triassic–Jurassic boundary, the last carbonate platform (Albenza Formation, Hettangian) developed. The Zu Limestone is lithologically similar and coeval with the Kössen Formation (Go-

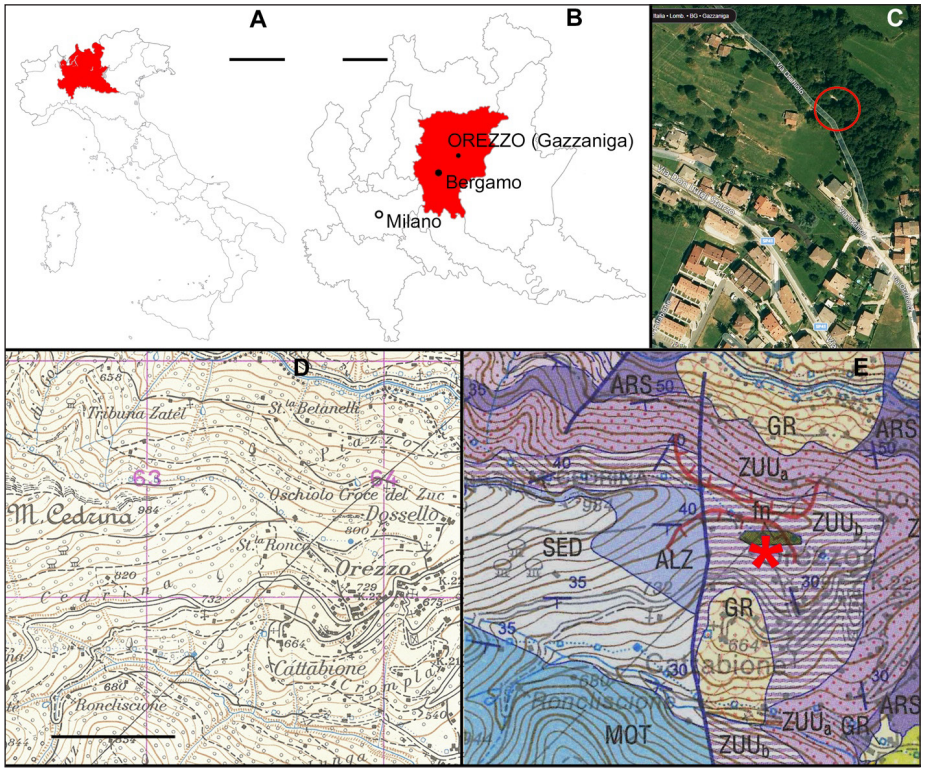

Fig. 1 - Fossil discovery site and geological setting: (A) Outline maps of Italy and Lombardy; (B) Outline maps of Lombardy and Bergamo Province, with the Gazzaniga Municipality; (C) Satellite view of the study area in Orezzo - Gazzaniga Municipality, with red circle indicating the discovery site; (D) topographic map excerpt from IGM 1:25.000 foglio 33 II-NO "Albino" (ed.1974); (E) excerpt not to scale from Carta Geologica d'Italia 1:50.000, foglio 077 "Clusone" (ISPRA 2012), the red asterisk indicates the fossil discovery site. Legend: (ARS) Riva di Solto Shale - *upper Norian*; (ZUUa lower lithozone, ZUUb upper lithozone) Zu Limestone - *Rhaetian*; (ALZ) Albenza Formation - *lower Hettangian*; (SED) Sedrina Limestone - *middle-upper Hettangian*; (MOT) Moltrasio Limestone - *Sinemurian*; (GR) Prato Grande Group - *Pleistocene*. Scale bars equal 200 km (A), 30 km (B), and 500 m (D).

lebiowski 1990), deposited in the Austroalpine Domain, equivalent to the Fraele Formation (Berra & Cirilli 1997), which outcrops in the Italian and Austrian Central Alps.

The Zu Limestone, ranging in thickness from 300 to 1,000 metres, is extensively exposed in the southern sector of the Orobic Alps (Gnaccolini 1965 and 1968). Various facies have been identified within this formation, allowing for its subdivision into two informal lithozones (Jadoul & Berra 2012). The lower lithozone (ZUUa) consists of cyclic alternations of black claystone, marl and dark grey micritic limestone. This lithozone culminates in a horizon (20-50 m thick on average) of massive, grey bioclastic packstone to framestone, frequently containing coral colonies. The upper lithozone (ZUUb) comprises cyclic alternations of ochre-grey marls, associated with marly limestone or predominantly micritic limestone. Towards the top of this lithozone, micritic limestone contains corals and, locally, megalodontids, while dark grey calcilutite marks its upper boundary (Malanotte Formation; Galli et al. 2007).

Litho-biofacies analysis suggests that the Zu Limestone was deposited in a subtidal to shallow marine environment with mixed terrigenous-carbonate sedimentation, and terrigenous input irregularly decreasing with time. This is characteristic of a carbonate platform-proximal slope system (Jadoul et al. 1994).

The Zu Limestone is generally highly fossiliferous, containing bivalve, brachiopod and coral assemblages that also include sponges, crinoids, algae, foraminifera, and occasional disarticulated vertebrate bone fragments. The presence of palynomorphs confirms a Rhaetian age for the formation (Cirilli S. in Jadoul et al. 1994).

At the discovery site (Fig. 1 A-D), slopes of the Seriana Valley connect to the valley floor via morphologies covered by extensive but discontinuous slope debris. A field survey conducted with Mr. Pio Carlo Brizzi confirmed that the specimen was found within natural slope debris, at the base of Zu Limestone outcrops.

In the area including the discovery site and across a wide surrounding territory, extending along the slope up to the ridge of Mount Cedrina, the CARG Sheet 077 Clusone (ISPRA 2012) reports outcrops belonging to the Zu Limestone. More specifically, these outcrops correspond to the formation's upper lithozone, ZUUb, which is characterised by cyclic alternance of fine-grained limestone and marl (Fig. 1E). This hypothesis is supported by examination of the rock matrix surrounding the specimen under a binocular microscope, that revealed that limestone enclosing the skull exhibits the same

lithological characteristics of the rocks outcropping on the mountain slope near the discovery site.

Considering the geographic, geomorphological and geological evidence at the discovery site, we conclude that the specimen most likely originates from the Zu Limestone. The Rhaetian age of this formation is entirely consistent with the chronostratigraphic distribution of placodonts in the Late Triassic.

Description of the specimen MCSNB 13033

The fossil has not undergone any preparation or restoration. It has a sub-spheroidal shape, broadly replicating the original arrangement of the skull bones. This results from natural weathering, with differing chemical and physical alteration of the calcareous matrix compared with the skull bones. The sediment enclosing the skull and completely filling the cranial cavities is generally softer than the bones themselves, causing the latter to appear slightly elevated in relief. The matrix displays compressive conchoidal fractures with rounded edges resulting from carbonate dissolution, whereas the bones exhibit impact cracks and abrasions caused by rolling contact at the most protruding points. As a result, the skull lacks the rostrum anterior to the orbits and most of the upper temporal arches. Although the orbital contours can be reconstructed, the natural margins of the orbits are mostly damaged and not complete.

As preserved, the specimen measures 6.3 cm in length and 6.1 cm in width. Its maximum height, from the highest point of the parietal skull table to the occlusal surface of the palatine tooth-plates, is 3.65 cm; the distance between the highest point of the parietal skull table and the palatal rami of the pterygoids is 3.46 cm and the height at the occiput, as preserved, is 3.08 cm (Tab. 1).

The following description is based on direct observation of the specimen and CT data. Several skull roof bones and their sutures are clearly visible on the surface, along with the large palatine tooth-plates and the contours of the maxillary tooth-plates in palatal view. Only a few remnants of other cranial elements are preserved externally, whereas CT data reveal partial preservation of the braincase, upper jaw bones, additional elements, and tooth replacement cavities—some of which contain unerupted tooth-plates.

Maximum skull length	6.3
Maximum skull width	6.1
Maximum skull height *	3.65
Height of the occiput as preserved	3.08
Minimum interorbital bridge width	0.6
Minimum intertemporal bridge width	1.8
Minimum orbit-upper temporal fenestra bridge width (right side)	0.73
Parietal foramen	0.71 x 0.43
Pterygoid palatal ramus length	0.80
Palatine length	3.61
Pterygoid palatal ramus length to palatine length	0.22
Rpl1	1.05 x 0.88
Rpl2	2.68 x 1.90
Lpl1	0.97 x 0.85
Lpl2	2.77 x 1.91
Rpl2/Rpl1 longitudinal diameter ratio	2.55
Lpl2/Lpl1 longitudinal diameter ratio	2.85
Rpl2 longitudinal/transverse diameter ratio	1.41
Lpl2 longitudinal/transverse diameter ratio	1.45

Tab. 1 - MCSNB 13033: measurements (cm) of the skull as preserved. *Measured from the highest point of the parietal skull table to the occlusal surface of palatine tooth-plates.

Dorsal view (Figs. 2C; 3C)

In dorsal view, as preserved, the skull exhibits wide, subcircular orbits circumscribed by the frontal, postfrontal, postorbital, jugal, and maxilla. The contribution of the prefrontal to their anterior margin cannot be assessed, as this bone is absent on both sides—a finding confirmed by CT data. Inside the orbits, CT slices reveal a posterolateral pillar extending between the skull roof and the palatines, composed of the postorbital, jugal, and palatine (Fig. 4G). Although the lateralmost portion of the jugal-postorbital suture is visible on both sides, the pillar itself is obscured by matrix filling the orbits.

The interorbital bridge appears almost entirely worn away, with bone exposed only along its margins and in the posteriormost region However, CT slices show a continuous yet very thin layer of bone between the orbits (Fig. 4K). We infer that this interorbital bridge was formed by the frontal(s), participating in the orbital dorsal margin (character 66). Despite the availability of CT data, it remains unclear whether the frontal bones were paired or fused. The minimum width of the interorbital bridge is 0.6 cm.

Fig. 2 - The skull of *Macroplacus raeticus* MCSNB 13033. Photographs of the specimen in left lateral (A), right lateral (B), dorsal (C), ventral (D), anterior (E), occipital (F) views. Scale bar equals 5 cm. Photos by Franco Valoti.

Only the anteromedial margins of the upper temporal fenestrae are preserved, formed by the postorbitals and the parietals. The bridge between the upper temporal fenestrae is entirely formed by the parietals, with a minimum width of 1.8 cm. The bridge separating the orbit from the upper temporal fenestra is preserved on both sides of the skull and is assumed to be formed by the postorbital (see "Re-examination of the holotype of *Macroplacus raeticus*, and comparison with MCSNB 13033 and *Psephoderma alpinum*"), with a minimum width of 0.73 cm on the right side.

The pineal foramen is displaced anteriorly on the parietal skull table, with frontal(s) not entering its anterior margin (character 10). It measures 0.71 cm in length and 0.43 cm in width based on CT slices in which its oval contour is fully visible.

A deeply interdigitating transverse suture, clearly separating the frontal(s) from two adjacent bones, is visible just posterior to the interorbital bridge. These two bones, medially fused along a tightly serrated suture, are identified as the postfrontals, following Schubert-Klempnauer (1975) (see "Re-examination of the holotype of *Macroplacus raeticus*, and comparison with MCSNB 13033 and *Psephoderma alpinum*"). On the right postfrontal, a radiating ossification pattern is evident, supporting the inferred sutural relationships. The paired postfrontals prevent direct contact between the frontal(s) and the parietals (character 13, new character 89).

The parietals contribute to a distinct lobate anterior process, which separates the postfrontals medially and meets them along deeply interdigitating sutures.

Lateral to the process, the postfrontals meet the parietals along deeply interdigitating sutures and form the posteromedial margins of the orbits. The posterolateral margins of the postfrontals extend

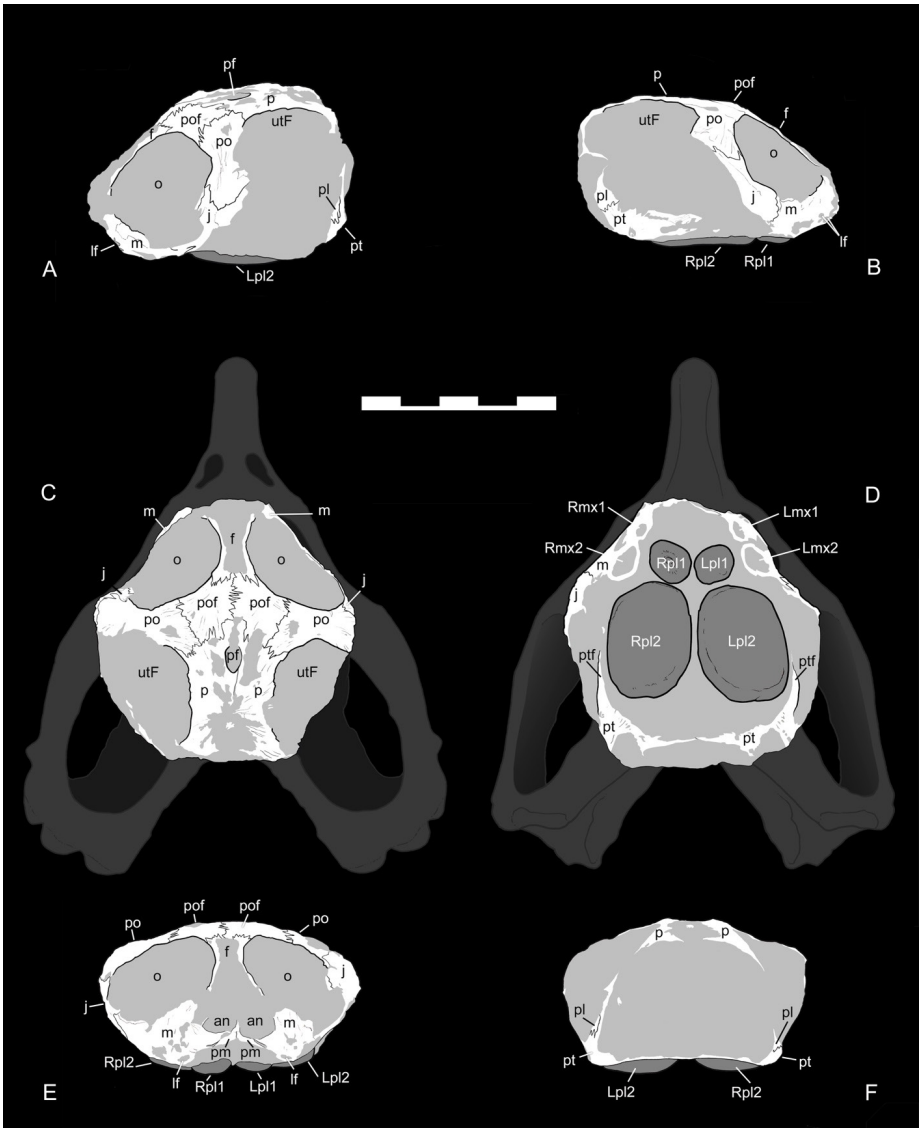

Fig. 3 - The skull of *Macroplacus raeticus* MCSNB 13033. Line drawings of the specimen in left lateral (A), right lateral (B), dorsal (C), ventral (D), anterior (E), occipital (F) views. The shaded outline of the whole skull in (C) and (D) is mainly based on the holotype of the species, the specimen SNSB-BSPG 1967 I 324; the outline of the rostrum is based on *Psephoderma*. Scale bar equals 5 cm. Drawings by Marco Auditore. See "Anatomical abbreviations" section above.

straight (character 15), establishing interdigitating sutural contact with the postorbitals. The postfrontals do not enter the upper temporal fenestrae due to the broad contact between the postorbitals and the parietals (character 16).

A straight suture extending posteriorly from the right posterolateral margin of the pineal foramen suggests that the parietals are paired elements—an interpretation unequivocally confirmed by CT data (Fig. 4E, H). The parietals are broad bones that form the entire skull roof between the upper temporal fenestrae. CT slices reveal that the parietal skull table is consistently thick throughout, even in areas that appear superficially corroded and infilled with matrix; a distinct layer of bone is visible in all anteroposterior transverse sections. Posterior to the pineal foramen, the parietals exhibit weak dermal ornamentation consisting of four low tubercular protuberances. Their well-preserved lateral margins are nearly straight, resulting in a weakly constricted skull table (character 14). No distinct step is present behind the pineal foramen. Anteriorly, the parietals contact the postfrontals medially and the postorbitals (sensu Schubert-Klempnauer 1975) laterally, along deeply interdigitating sutures. The parietals do not form distinct anterolateral processes that are entirely embraced by the postfrontals (character 12). We assume that the posterior margin of the skull table is relatively well preserved, as evidenced by the clear presence of laterally diverging squamosal processes of the parietals, despite their truncation at the base. The contacts between the parietals and the occipital elements cannot be determined, as the latter are not preserved (see below; Figs. 2F; 3F). CT data revealed the presence of descending parietal processes suturing to the epipterygoids (see "Braincase", Fig. 4H).

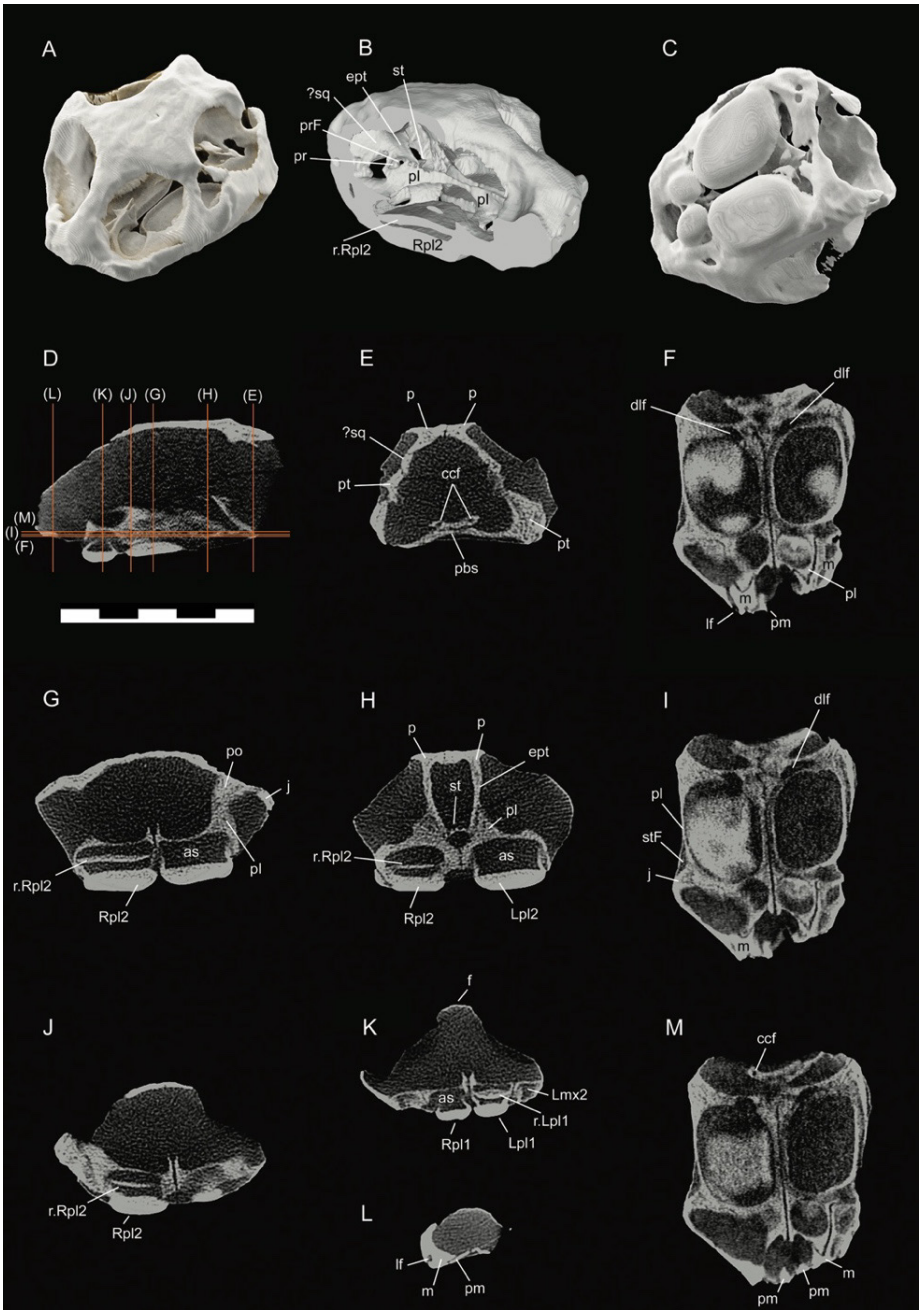

Fig. 4 - CT scanning of the skull of *Macroplacus raeticus* MCSNB 13033. 3A, 3B, 3C - three-dimensional model of the skull of *Macroplacus raeticus* MCSNB 13033 generated from CT scan in left anterodorsolateral view (A), right anterodorsolateral view with the lateral side removed to expose the internal bones (B), and right posteroventrolateral view. 3D - union framework of the horizontal (F, I, and M) and transverse (E, G, H, J, K, L) slices reported on the midsagittal slice. Horizontal slices: M, slice 305; I, slice 309; F, slice 312. Transverse slices: E, slice 100; H, slice 147; G, slice 215; J, slice 250; K, slice 280; L, slice 344. In the transverse slices the skull is seen in anterior view, and in horizontal slices it is seen in dorsal view, therefore the left side of the figure from E to M is the right side of the animal, and vice versa. See "Anatomical abbreviations" section above.

The postorbitals are large bones that form the bridges between the orbits and upper temporal fenestrae, contributing to the posterior margins of the orbits and the anterior margins of the upper temporal fenestrae. Their medial margin contacts the postfrontal anteriorly and the parietal posteriorly, along interdigitating sutures (see "Re-examination of the holotype of *Macroplacus raeticus*, and comparison with MCSNB 13033 and *Psephoderma alpinum*"). Their lateral margins contact the jugal. CT data revealed that a descending process of the postorbitals contributes to the posterolateral pillar inside the orbit (Fig. 4G). However, although the epipterygoid is preserved on both sides in MCSNB 13033 (see "Braincase"), it was not possible to determine whether the postorbital formed a medioventral process abutting the lateral surface of that bone at the posterodorsal margin of the foramen interorbitale (character 21). The contribution of the postorbitals to the upper temporal arches remains unknown, as these are not preserved in MCSNB 13033.

Lateral views (Figs. 2A-B; 3A-B)

Limited additional information is available from the lateral views, as the upper temporal arch-

Tab. 2 - Dental and palatal comparative measurements (cm and cm^2) and ratios.*As Rpl2 is not preserved we assumed it was the same size as Lpl2.

	MCSNB 13033	*Macroplacus* SNSB-BSPG 1967 I 324	*Psephoderma* MSNM V471
Palate length (palatine+pterygoid)	4.30	8.65	4.75
Palate width (distance between the medial margins of the subtemporal fossae)	4.25	10.18	4.09
Area of the palate (palate length x palate width)	18.27	88.06	19.42
Longitudinal diameter Rpl1	1.05	2.33	0.76
Transverse diameter Rpl1	0.88	2.04	0.64
Longitudinal diameter Lpl1	0.97	2.08	0.78
Transverse diameter Lpl1	0.85	1.88	0.65
Longitudinal diameter Rpl2	2.68	–	2.44
Transverse diameter Rpl2	1.90	–	1.69
Longitudinal diameter Lpl2	2.77	6.84	2.54
Transverse diameter Lpl2	1.91	4.85	1.71
Area of Rpl1 and Lpl1	0.92 0.82	4.75 3.91	0.49 0.51
Area of Rpl2 and Lpl2	5.09 5.29	– 33.17	4.12 4.34
Area of right + left palatine tooth-plates (Pl1+Pl2)	10.38	75.00*	9.46
Palate area / Pl1+Pl2 area	1.49	1.17	2.05
Palate area / Rpl2+Lpl2 area	1.76	1.33	2.29

es, quadrates, and squamosals are either completely missing or only fragmentarily preserved. On both sides, only the anterior portions of the postorbital and jugal are sufficiently preserved, with a distinct suture between them. Anteriorly, these elements form the posterior half of the orbital margin. Posteriorly, the shape of the postorbitals and jugals, as well as their relationships with the bones forming the temporal arches, cannot be determined.

Slightly posterior to the midpoint of the orbital longitudinal diameter, the jugals contact the maxillae (character 18). The suture is more clearly visible on the right side (Figs. 2B; 3B), where the maxilla is better preserved, with the tip of the jugal extending anteriorly along the ventral margin of the orbit. It reaches close to—but remains behind—the midpoint of the longitudinal diameter of the orbit (character 8). Anterodorsal to the anterior maxillary tooth-plate, a labial foramen for a cutaneous branch of the superior alveolar nerve is distinctly visible on the right maxilla (Figs. 2B; 3B).

On both sides, part of the suture between the palatine and the quadrate ramus of the pterygoid is clearly visible.

Ventral view (Figs. 2D; 3D; 4C, F-K, M)

The bones forming the hard palate are only minimally exposed in the fossil, but CT data reveal more extensive preservation of the various elements and their sutural contacts.

In ventral view, the most distinguishing feature is the presence of two rounded palatine tooth-plates per side (characters 36 and 37), exposed due to chemical alteration of the matrix. The posterior palatine tooth-plates (Rpl2 and Lpl2) are massive, dwarfing the already large anterior ones (Rpl1 and Lpl1), with a ratio of posterior to anterior palatine tooth-plate maximum lengths of 2.55 on the right side and 2.85 on the left (Tab. 1). The ratio of longitudinal to transverse diameter of the posterior palatine tooth-plates is greater than 1.4 (character 38) (Tab. 1).

The tooth-bearing palatine bones are embedded in the limestone matrix but are well preserved, as revealed by CT data (Fig. 4). They form most of the hard palate, meeting in a medial suture (character 60), and their surfaces are almost entirely occupied by Rpl2 and Lpl2 (Tab. 2; see "Re-examination of the holotype of *Macroplacus raeticus*, and comparison with MCSNB 13033 and *Psephoderma alpinum*").

Only a very thin portion of the palatal rami of the pterygoids is visible, joining along a median suture to form the posterior portion and margin of the hard palate. Laterally, on both sides, the strongly abraded pterygoid flanges are identifiable near the posterior margins of Rpl2 and Lpl2, along with

the posterolaterally projecting quadrate rami of the pterygoids. CT data reveal the full palatal exposure of the pterygoids (palatal rami), which are significantly shorter than the palatines (character 61) (Fig. 4C, F, I, M), with a length-to-palatine ratio of 0.22 as measured in CT slices (character 44).

Very wide dental lamina foramina are visible in CT scans, opening just posterior to pl2 along the contact between the palatines and the palatal rami of the pterygoids (Fig. 4C, F, I, M), allowing ectodermal tissue to grow into the replacement cavities (*sensu* Rieppel 2001a) Lateral to these foramina, the palatines and pterygoids form the vertical lateral wall of the alveolus, which is very thin. CT scans also reveal large replacement cavities or alveolar spaces (*sensu* Neenan et al. 2014) inside the palatines, beneath the erupted tooth-plates, dorsally roofed by a thin layer of bone.

A replacement tooth-plate at development stage 2 (sensu Neenan et al. 2014) is clearly visible inside the alveolar space of Rpl2 (Fig. 4B, G, H, J). The erupted Rpl2 is smaller than the erupted Lpl2, has a worn crushing surface, and exhibits a uniform texture. In contrast, Lpl2 is larger, having erupted more recently—consistent with ongoing growth at the time of death—and still retains a sculptured surface. Notably, this sculptured crushing surface is distinctly delimited from a larger smooth "base," which was likely the portion of the tooth-plate enclosed within the palatal soft tissues. A second replacement tooth-plate, at an advanced stage of development 2, is visible in the alveolar space of Lpl1 (Fig. 4K), which has a worn surface. In contrast, the larger Rpl1 exhibits a distinctive unworn ornamentation, featuring a central cusp emerging from the bottom of a shallow pit, itself encircled by a radially wrinkled relief.

The sutural relationships of the bones forming the hard palate are clearly visible in CT slices. The palatines contact the maxillae laterally and anterolaterally along a V-shaped suture, while their notched anteromedial margins define the posterior border of the internal nares (Fig. 4F, I, M). Medially, the palatines project into short, pointed processes for articulation with the vomers, which, however, are not preserved. The posteriormost portions of the premaxillae are visible, articulated with the maxillae (Fig. 4F, I, M). Thus, the internal nares were bordered anteriorly by the premaxillae, posteriorly by the palatines, laterally by the maxillae, and medially by the vomers (character 42).

In the palatal aspect of the fossil, the maxillae are partially exposed laterally, each originally bearing two tooth-plates (character 35). These tooth-plates were likely lost due to physical breakdown (see above), but their respective alveoli remain distinct, rimmed by a layer of attachment bone that originally ankylosed the functional tooth-plate roots to the alveolar wall (sensu Rieppel 2001a) (Fig. 2D). CT data confirm the absence of the maxillary tooth-plates and the damage to the lateralmost portion of the maxillae. Alveolar spaces of the maxillary tooth-plates are visible in CT scans but do not contain any replacement teeth (Fig. 4K).

As noted above, only the very bases of the premaxillae appear to be preserved, though incompletely, in CT slices, along with their contact with the maxillae on the hard palate (Fig. 4F, I, M). CT scans indicate that a process of the maxilla extends anteriorly into the rostrum in ventral view (character 39) (Fig. 4F). For details regarding the presence or absence of premaxillary teeth (character 32), see "Re-examination of the holotype of *Macroplacus raeticus*, and comparison with MCSNB 13033 and *Psephoderma alpinum*".

Finally, CT data reveal the preserved right jugal at its contact with the palatine and maxilla on the hard palate, confirming the absence of the ectopterygoid in MCSNB 13033 (character 43). The jugal does not extend posteriorly along the anteromedial margin of the subtemporal fossa (character 9) (Fig. 4I).

Anterior view (Figs. 2E; 3E; 4L)

In anterior view, it is most evident that the skull was fractured at the very base of the rostrum, just posterior to the retracted external nares or aperturae nasi osseae (character 65). Their floor is primarily formed by the premaxillae and laterally completed by the maxillae (Fig. 3E), which contribute to the ventrolateral wall of the nasal opening (character 7).

The rod-like premaxillae meet medially, and due to their shape, they form a ventrally concave rostrum (character 40), with a single longitudinal groove (character 41) that is V-shaped in transverse section (Figs. 2E; 3E). CT data confirm the preservation state of the premaxillae and their contact pattern with the maxillae, with the maxillae dorsally overlapping the premaxillae to some extent in transverse section (Fig. 4L). The bones posterior to the

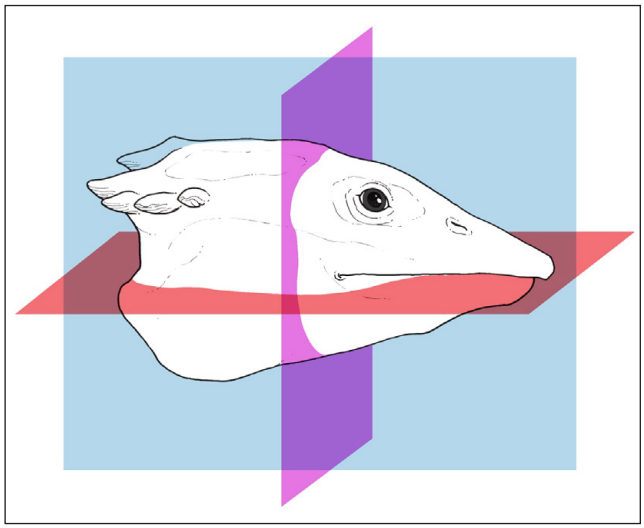

Fig. 5 - The head of *Macroplacus raeticus*, showing the three anatomical planes used to describe the anatomy of the specimen MCSNB 13033 and its CT slices: 'midsagittal plane' (blue); 'horizontal plane' (red); and 'transverse plane' (purple). Drawing by Marco Auditore.

nares—presumably the posterior portion of the premaxillae, prefrontals, and nasals—are not preserved.

Posterior view (Figs. 2F; 3F; 4C)

As preserved, the posterior view of the specimen provides no anatomical information, as the area corresponding to the occiput is entirely filled with matrix. CT data reveal no preservation of the bones that circumscribed the foramen magnum and formed the occipital condyle—specifically, the supraoccipital, basioccipital, and exoccipitals. The absence of these elements exposes the basicranium, which is formed by the parabasisphenoid complex (see "Braincase").

Braincase (Fig. 4A-B, D-E, H, M)

CT data reveal that some elements of the braincase are preserved in MCSNB 13033. As in all cyamodontoid placodonts, the braincase is predominantly ossified, forming an akinetic structure including elements of the neurocranium, skull roof, and splanchnocranium.

The basicranium is formed by the parabasisphenoid complex. The basisphenoid appears to be fused to the palatal rami (and presumably to the quadrate rami, though this is unclear) of the pterygoids. More anteriorly, it is fused to the palatines (basipterygoid articulation sensu Nosotti & Pinna 1993), prootics and epipterygoids. In the sphenoid region, medial to the epipterygoids, the braincase floor is perforated by paired foramina through which the cerebral carotids entered the cranial cavity (Fig. 4E, M). CT slices show that these foramina are the openings of two canals running inside the basicranium, transmitting the internal carotid arteries forward from the occiput. These foramina typically open near the hypophyseal seat or sella turcica (Fig. 4D-E, H).

Anterior to the hypophyseal region, the raised, converging medial margins of the palatines meet to form a V-shaped groove for the insertion of the interorbital septum (Fig. 4B, G, J, K). The expected presence of a pteroccipital foramen cannot be confirmed unequivocally, nor can the spatial relationship between this foramen and the post-temporal fenestra (character 30). In the three-dimensional model derived from CT data, the prootics are exposed in posterior view (character 31).

In the sphenoid region of the braincase, both epipterygoids are preserved, extending between the parietals and the palatines and forming most of the ossified wall of the braincase (Fig. 4B, H). Their state of preservation and ossification is difficult to assess, particularly given the early ontogenetic stage of this individual. An epipterygoid fossa (sensu Nosotti & Pinna 1996) is not visible (character 25). CT slices indicate that the descending flanges of the parietals, which join the broad (character 19) dorsal processes of the epipterygoids, were not very deep (Fig. 4H; character 20).

Ventrally, the epipterygoids abut exclusively against the palatines (Fig. 4B, H) due to the substantial posterior development of the latter (Fig. 4C, F, I, M). In the three-dimensional skull model, the epipterygoids appear thin and not thickened ventrally, providing no indication of a palatoquadrate cartilage recess in this region (character 27). The posterior concave margin of the epipterygoid, together with the prootic, defines the lateral opening of the cavum epiptericum, i.e., the prootic fenestra (Fig. 4B). Whether the epipterygoid contacted the squamosal dorsal to the post-temporal fenestra in MCSNB 13033 (character 24) cannot be established unequivocally, as the posterior portion of the temporal fossae is only partially preserved and difficult to interpret.

The prootics are visible on both sides of the skull, transversely oriented. Like the epipterygoids, the prootics ventrally abut exclusively against the palatines (Fig. 4B).

Posterior to the prootics, the preservation state of the squamosals is unclear. An otic, neomorphic process of the squamosals meeting the prootics is not visible (character 26), and the contours and size of the post-temporal fenestrae cannot be determined with certainty (character 46) (Fig. 4B).

Given the challenges involved in generating the three-dimensional model from CT data (see "Materials and Methods"), the interpretation and detailed description of the braincase in the model itself remain difficult.

Re-examination of the holotype of *Macroplacus raeticus*, and comparison with MCSNB 13033 and *Psephoderma alpinum* (Figs. 2-3; 6-8; S1; S2)

The holotype and, to date, the only known specimen of *Macroplacus raeticus*, SNSB-BSPG 1967 I 324, is a three-dimensionally preserved, isolated skull from the Rhaetian of the Bavarian Alps (Fig. S1). The anatomical study of this specimen, originally described by Schubert-Klempnauer (1975, figs. 1-5), has been challenging over the years due to issues such as over-preparation, some compression, and deformation (Rieppel 2000a, fig. 24 and 2001b, fig. 26; Wang et al. 2019b). For a historical overview of previous research and additional references, see "Supplementary contents".

After a thorough re-examination of the fossil (SN), we found new evidence requiring a partial revision of earlier interpretations (Fig. 6). This section describes and discusses previously unreported or revised anatomical features of the *Macroplacus raeticus* holotype, comparing it with the new specimen MCSNB 13033 and the skull of *Psephoderma alpinum*. *Macroplacus* and *Psephoderma* are the only placodonts known to have lived during the latest Triassic (Rhaetian) and are considered the longest-surviving representatives of Placodontia (Neenan et al. 2015).

Psephoderma alpinum is one of the best-known armoured placodonts, represented by numerous specimens (Pinna 1976a, 1976b, 1978, 1979, and 1980a, b; Pinna & Nosotti 1989; Renesto & Tintori 1995; Rieppel 2000a and 2001b; Neenan & Scheyer 2014). It is typical of the Norian and Rhaetian of the Alps, with additional remains described from the Rhaetian of England (Meyer v. 1858a, b; Storrs 1994). Both fragmentary remains and complete, articulated skeletons have been found in the upper Norian deposits of the Orobic Alps (Bergamo Province, northern Italy) in the outcrops of the Zorzino Limestone Formation (Pinna & Nosotti 1989; Renesto & Tintori 1995).

Well-preserved three-dimensional skulls of *Psephoderma alpinum* provide an excellent basis for comparison. One such specimen, from the Kössen Formation at Schesaplana Mountain, Switzerland (PIMUZ A/III 1491), was described by Neenan & Scheyer (2014). The three-dimensionally preserved skull MSNM V 471 (Fig. S2), originally described by Pinna (1976a, figs 2–7, plates I–III) and later referenced by Rieppel (2000a, fig. 27 and 2001b, figs 28–29), was re-examined (SN) for this study. The specimen originates from the Lower Rhaetian Riva di Solto Shale Formation at Monte Cornizzolo (Lombardy, northern Italy) (Pinna 1976a). Given its state of preservation, it provides a valuable point of comparison with the *Macroplacus raeticus* holotype. Unless otherwise specified, the following descriptions and comparisons concerning the species *Psephoderma alpinum* refer to this specific specimen.

Cranial architecture, palatal morphology and tooth-plate proportions.

The cranial morphology of the holotype of *Macroplacus raeticus* exhibits extreme specialisation for durophagy. Among the Cyamodontoidea, *Macroplacus* possesses the largest palatal tooth-plates relative to its palate size and exceptionally wide upper temporal fenestrae, suggesting powerful, well-developed adductor muscles that maximized its jaw-crushing efficiency.

When compared to skull specimens of *Psephoderma* (Pinna 1976a; Rieppel 2000a, 2001b; Neenan & Scheyer 2014) (Fig. S2), the holotype of *Macroplacus* (Figs. 6; S1) does not reveal substantial differences in overall skull proportions. However, *Macroplacus* and *Psephoderma* can be readily distinguished by a unique combination of characters related to skull morphology, the tooth-plate arrangement and relative proportions—both among the tooth-plates themselves and in relation to the bones forming the palatine vault.

As MCSNB 13033 (Figs. 2–3) lacks both the rostrum and the temporal arches, its overall preservation is less complete than that of either *Macroplacus* or *Psephoderma* specimens. However, when scaled to the skull size of the *Macroplacus* holotype,

many proportions appear consistent, as confirmed by comparisons of measurements of cranial bones and tooth-plates (see below; Tab. 2).

Although the total skull length of the *Macroplacus* holotype cannot be measured due to the incomplete rostrum, we determined that the ratio of skull total length to total height exceeds 3 (see discussion of character 2, newly coded for *Macroplacus* in this study). This aligns *Macroplacus* with the Placochelyida—characterised by a more longitudinally elongated skull and a less arched skull roof than in Cyamodontida (Schubert-Klempnauer 1975, fig. 8). The ratio places *Macroplacus* between *Placochelys* (2.55) and *Psephoderma* (3.29), the latter likely affected by taphonomic compression. A value greater than 3 remains valid even when adjusting the total height of the slightly compressed holotype skull using MCSNB 13033, which appears to retain its original proportions.

As noted by Rieppel (2001b, figs. 28 and 29), the skull of *Psephoderma* (Fig. S2) is relatively narrow, with upper temporal fenestrae that are proportionally short and distinctly narrower than in other cyamodontoids. Additionally, the disproportionality between the orbits and upper temporal fenestrae is greater in *Macroplacus* than in *Psephoderma* (Rieppel 2001b, tab. 8). Nevertheless, the ratio of the longitudinal diameter of the upper temporal fenestra to the orbital longitudinal diameter (character 23) falls within the same range for both taxa, remaining less than 2. A comparison with MCSNB 13033 is not possible, as its temporal arches are entirely missing.

There is strong, albeit indirect, evidence for an edentulous rostrum formed by the premaxillae in the *Macroplacus* holotype skull (Fig. 6). According to Schubert-Klempnauer (1975, fig. 6; see also "Supplementary contents" in this paper), a key argument supporting this interpretation is that the preserved portion of the holotype's premaxillae is toothless, with no alveoli visible at the very base of the broken rostrum. Additionally, the preserved portion of the rostrum in the holotype skull suggests it was composed of juxtaposed, rod-like premaxillae (Schubert-Klempnauer 1975, fig. 6), forming a median groove or concavity on the ventral surface of the rostrum. This morphology is entirely consistent with that observed in Placochelyida, whereas Cyamodontida typically possess a rounded snout formed by short, broader premaxillae (character 3). In placochelyids, a fully preserved rostrum is invariably toothless, whereas cyamodontid placodonts exhibit the opposite condition.

Unlike *Placochelys* (Rieppel 2001b, figs. 1–10), the rostrum of *Psephoderma* is not downturned (Fig. S2D, F). Consequently, in lateral view, the crushing surface of the palatal tooth-plates and the ventral surface of the rostrum lie on the same horizontal plane—indicating that the roof of the mouth is flat (see discussion under character 4). Based on the preserved base of the rostrum, the skull of the *Macroplacus* holotype also exhibits a flat palatal roof (Fig. S1D). As previously noted by Schubert-Klempnauer (1975, fig. 8; see also "Supplementary contents" in this paper), a comparison of *Cyamodus*, *Placochelys*, and *Macroplacus* reveals that the reduction—or more precisely, the absence—of premaxillary dentition in *Placochelys* is associated with a less arched palatal vault (flat in *Psephoderma* and *Macroplacus*) than in *Cyamodus*. In *Cyamodus*, this arch is anteriorly completed by procumbent premaxillary dentition, whereas in *Placochelys* it is formed by the downturned edentulous rostrum. According to Schubert-Klempnauer (1975), the progressive flattening of the palatal roof, including the masticatory surface and rostrum, in *Placochelys* and *Macroplacus* has functional significance: the rostrum (and potentially an overlying horny beak) would have been shaped to optimise performance in combination with the levelling of the tooth-plate surfaces (Schubert-Klempnauer 1975).

Observations of the *Psephoderma* skull (Fig. S2) suggest that the rostrum of *Macroplacus* was likewise elongated, straight in lateral profile, and edentulous (Fig. 6). This hypothesis aligns with Rieppel's statement that "elongation of the rostrum [in Placochelyida] is correlated with a reduction of its dentition, until the rostrum becomes an edentulous, elongate and narrow structure in the apomorphic representatives of the clade (*Placochelys*, *Psephoderma*)" (Rieppel 2002a). As noted, *Macroplacus*, along with *Psephoderma*, represents the latest occurrence of placodonts in the fossil record and exhibits a highly specialised morphology, closely resembling that of *Psephoderma* in many respects.

It is also noteworthy that the rostrum of placochelyids is invariably ventrally concave, and in some cases—such as in *Psephoderma*—bears distinct grooves leading to the internal nares (Rieppel 2001b) (Fig. S2C). From a functional perspective, these morphologies correspond to differing feeding

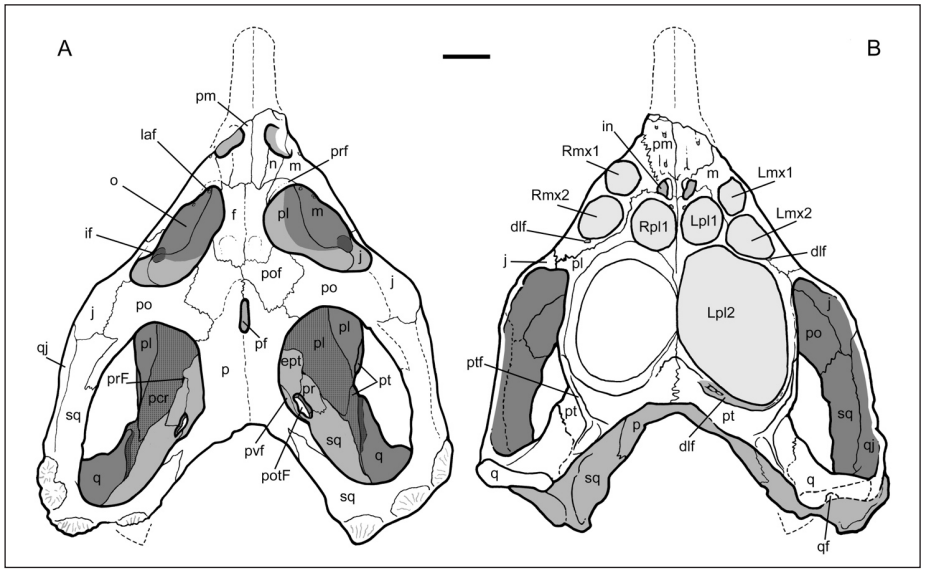

Fig. 6 - Reconstruction of the holotype of *Macroplacus raeticus*, in dorsal (A) and ventral (B) view. In (A), the dotted area indicates the palatoquadrate cartilage recess. The figure is redrawn and modified from Schubert-Klempnauer (1975). The outline of the rostrum is based on *Psephoderma*. Scale bar equals 2 cm. Drawings by Marco Auditore. See "Anatomical abbreviations" section above.

mechanics and strategies (Rieppel 2002a; Gere et al. 2024). These considerations align with the methodological framework proposed by Bryant & Russell (1992), which allows inference of unpreserved osteological and non-osteological features based on the cladistic distribution of known characters in related taxa. Where necessary, this method involves selecting among equivocal or conflicting phylogenetic inferences by considering form-function correlations and ecological affinities among taxa.

The rostrum in MCSNB 13033 cannot be directly assessed, as the skull is broken posterior to the external nares. However, as in the holotype of *Macroplacus*, it consists of rod-like premaxillae and is ventrally concave, featuring a single median longitudinal groove (see description of MCSNB 13033, anterior view, Figs. 2E; 3E). Additionally, the masticatory surface formed by the palatal dentition in MCSNB 13033 is flat. Following the methodological framework of Bryant & Russell (1992) outlined above, we infer that MCSNB 13033 most likely possessed an elongated, edentulous rostrum, as observed in all well-preserved representatives of Placochelyida.

Assuming that the holotype of *Macroplacus* possessed an edentulous rostrum, the preserved tooth-plates in the skull would represent the complete upper dentition, with a dental formula of two palatine and two maxillary tooth-plates per side—the same as in MCSNB 13033 and *Psephoderma alpinum*.

However, compared with the holotype of *Macroplacus* and MCSNB 13033, *Psephoderma* exhibits differences in tooth-plate proportions and shape (Fig. S2; Tab. 2). Unlike in *Psephoderma*, the posterior palatine tooth-plates (pl2) in the holotype of *Macroplacus* are hypertrophic (Schubert-Klempnauer 1975; Rieppel 2001b) and, due to the extremely shortened pterygoids (see below), are positioned very close to the ventral flanges of the pterygoids (Figs. 6; S1). Additionally, the palatine and maxillary tooth-plates are tightly packed (Schubert-Klempnauer 1975), covering the entire extent of the hard palate. Lastly, in the holotype of *Macroplacus*, pl1 and mx2 are approximately the same size, whereas in *Psephoderma*, pl1 is distinctly smaller than mx2.

To quantify the hypertrophy of pl2, we calculated the area of the palatal surface—primarily formed by the palatines and the palatal rami of the pterygoids—by multiplying the maximum length of the hard palate (from the posterior margin of the palatal rami of the pterygoids to the anteriormost extent of the palatines) by its maximum width (the distance between the medial margins of the subtemporal fenestrae). The area of the palatine tooth-plates was estimated by multiplying their maximum length by their maximum width, approximating their surface as rectangular or square (Tab. 2).

These values were used to calculate the ratio of the palatal surface area to the palatine tooth-plates area, which is 2.05 for *Psephoderma* and 1.17 for the *Macroplacus* holotype. Additionally the ratio of the palatal surface area to the total area of pl2 is 2.29. for *Psephoderma* and 1.33 for *Macroplacus* (Tab. 2). These results highlight the clustering of tooth-plates on the hard palate and the extremely large size of pl2 in the *Macroplacus* holotype.

Superimposed, at-scale dorsal views of the holotype of *Macroplacus* and MCSNB 13033 reveal minor but notable differences in the proportions of some palatal bones in ventral view. In MCSNB 13033, structures such as the palatines and their large posterior palatine tooth-plates (pl2), are approximately 90% the size of those in the holotype. The ratios are 1.49 for the palatal surface to total pl1+pl2 area, and 1.76 for the palatal surface to total pl2 area (Tab. 2), representing intermediate values between *Psephoderma* and the holotype of *Macroplacus*. Compared with the holotype, MCSNB 13033 exhibits less hypertrophied pl2. However, when compared with the *Psephoderma* specimen MSNM V 471—of approximately the same size—pl2 in MCSNB 13033 are clearly larger relative to the palatal surface. These differences may reflect individual variation or positive allometry, as the palatine tooth-plates are proportionally larger in the holotype of *Macroplacus*, which is approximately twice the size of MCSNB 13033. The jaw apparatus appears to have been well developed and powerful even in small, juvenile individuals such as MCSNB 13033, but became increasingly robust during ontogeny. Indeed, Rieppel (2001b) hypothesised that "given the relatively large size of the skull of *Macroplacus*, the hypertrophy of the posterior palatine tooth-plates may be the result of their positive allometric growth" (as he also proposed for *Psephoderma*). On these grounds, Pinna (1978, 1989, 1990, and 1999) speculated that *Macroplacus* represented a later ontogenetic stage of *Psephoderma*, suggesting synonymy of the two taxa at the genus level (see "Supplementary contents").

We conclude that hypertrophic pl2 is a diagnostic feature of MCSNB 13033, shared with the holotype of *Macroplacus* (Schubert-Klempnauer 1975; Rieppel 2000a and 2001b).

Regarding the shape of pl2, measured by the ratio of the longitudinal to the transverse diameter of the posterior palatine tooth-plate (character 38), this trait varies among cyamodontoid taxa (Rieppel 2001b, p. 67, tab. 7). With ratios of 1.41 in the holotype of *Macroplacus* and 1.4–1.5 in adult *Psephoderma* specimens, Rieppel concluded that both taxa possess elongated pl2. However, the holotype of *Macroplacus* exhibits quadrangular-shaped Lpl2 (Rpl2 is not preserved), in contrast to the distinctly oval pl2 of *Psephoderma*. Additionally, as noted above, pl2 in *Macroplacus* cover most of the palatal surface, unlike in *Psephoderma* (specimens MSNM V 471 and PIMUZ A/III 1491). In MCSNB 13033, the ratio of the longitudinal to the transverse diameter of the posterior palatine tooth-plates is 1.41–1.45, closely matching that of the holotype of *Macroplacus*, despite differences in size and ontogenetic stage (Tab. 2). While the shape of pl2 in MCSNB 13033 is not quadrangular as in the *Macroplacus* holotype, it is also not as oval and elongated as in *Psephoderma*.

In this context, we note that Rieppel (2001b, tab. 7) based his measurements for *Psephoderma alpinum* on specimen MSNM V 471, considering it representative of the adult ontogenetic stage of the species. However, larger specimens exist—such as the fully preserved ST82903 described by Renesto & Tintori (1995; erroneously reported therein as ST82003)—now housed in the Soprintendenza ABAP Bergamo-Brescia (Ministero della Cultura, Italy) fossil depot in the Comune di Zogno (Bergamo, Italy). The overall skull length of this specimen, measured from the tip of the rostrum to the occipital condyle, is 15.5 cm (Renesto & Tintori 1995, tab. 1), exceeding that of MSNM V 471 (10.0 cm). Despite the specimen being exposed dorsally, Renesto & Tintori (1995) reported two large, flat tooth-plates on the mandibles, as well as on the maxillae and palatines. The posterior palatine tooth-plates were described as "enormously developed", but were neither figured nor measured. Unfortunately, we were unable to examine this specimen directly and thus could not compare the size of pl2 in ST82903 with that of MSNM V 471.

Another distinctly larger specimen—approximately one-third larger than MSNM V 471, according to Pinna (1976a)—is the mostly incomplete skull ST2014.58.83, now stored in the same fossil depot in Zogno. This specimen was originally described by Boni (1946 and 1948, figs. 1–4) as *Placochelys malanchinii*, later reassigned by Pinna (1976a, fig. 8, plates IV–V) to *Placochelyanus stoppanii*, and finally attributed to *Psephoderma alpinum* (Pinna 1978). Despite its larger size, ST2014.58.83 exhibits a ratio of the longitudinal to the transverse diameter in the posterior palatine tooth-plate of 1.56 (36.14 × 23.22 mm, measured from a cast of the specimen), only slightly higher than that of MSNM V 471.

Finally, we note that the type specimen of *Psephoderma alpinum* (Meyer v. 1858a, b; Nosotti & Pinna 1989) is a large, isolated carapace (length 37.5 cm, width 42.3 cm as preserved), suggesting that

its skull was likely comparable in size to ST82903 (Renesto & Tintori 1995). Given that the largest *Psephoderma* specimens are approximately one and a half times the size of the "adult" specimens used by Rieppel (2001b) in his comparisons, we assume that inclusion of these larger forms would not alter our conclusions.

In the *Macroplacus* holotype skull, the pterygoids are fully preserved and exhibit marked anteroposterior shortening (character 61). In contrast, the palatines are exceptionally broad, forming the majority of the palatal surface. The ratio of the pterygoid palatal ramus ("palatal exposure") length to the palatine length is 0.17 (see discussion under character 44), while in MCSNB 13033, it is 0.22 (Tab. 1). A ratio below 0.3 is unique within Placochelyida and underscores the pronounced pterygoid shortening in these two specimens.

For comparison, in *Psephoderma* specimen MSNM V 471 the ratio is 0.36, exceeding 0.3. It is reasonable to infer that the shortening of the pterygoids relative to the palatines in the holotype of *Macroplacus* and in MCSNB 13033 is associated with the development of their enlarged posterior palatine tooth-plates (see also Rieppel 2001b).

However, it is important to note that shortened pterygoids relative to the palatines—and a ratio below 0.3—also occur in *Protenodontosaurus*, yet without the presence of hypertrophic palatine tooth-plates. The same applies to *Cyamodus kuhnschnyderi*, where the ratio ranges from 0.2 to 0.3 (Rieppel 2001b, p. 38).

Dorsal view (Figs. 6A; S1A)

We concur with Rieppel (2000a, fig. 24A and 2001b, fig. 26B) regarding the identification of the nasals and prefrontals in the *Macroplacus* holotype, which were previously interpreted as the prefrontals and lacrimals by Schubert-Klempnauer (1975). According to Schubert-Klempnauer, paired, rectangular nasals that contacted each other medially (character 6) formed approximately half of the interorbital bridge, with the remainder formed posteriorly by the frontals (Schubert-Klempnauer 1975, fig. 1). However, he illustrated the nasal-frontal suture only on the right side of the specimen. In our view, this interpretation is highly doubtful, and Rieppel's identification—where Schubert-Klempnauer's "nasals" correspond to the prefrontals—is considerably more plausible. In the *Macroplacus* holotype, the nasals are not in contact along the midline of the skull (character 6), and the interorbital bridge is almost entirely formed by the frontals, with only negligible contribution from the prefrontals. This condition, in which the nasals remain separate, is shared with other Placochelyida, including *Psephoderma*, the Chinese genus *Psephochelys*, and the highly specialised cyamodontoid *Henodus*. As for the lacrimal bone, it is now universally accepted that lacrimals are absent in placodonts—and more broadly within Sauropterygia (see Rieppel 2000a)—further supporting Rieppel's identification of this element as the prefrontal in the *Macroplacus* holotype. Neither the nasals nor the prefrontals are preserved in MCSNB 13033. We concur with previous authors in describing the frontal of the *Macroplacus* holotype as a paired bone, whereas CT slices suggest the opposite in MCSNB 13033 (see above, Fig. 4K).

We disagree with Rieppel's (2001b) description of the frontal as conspicuously widening posterior to the orbit—a feature not observed in any other cyamodontoid placodont. His interpretation incorporates the postfrontal sensu Schubert-Klempnauer (1975) within the frontal. Instead, we concur with Schubert-Klempnauer's identification of transverse sutures representing the contact between the frontals and the postfrontals in the *Macroplacus* holotype. These sutures are even more clearly visible in MCSNB 13033 (Figs. 2C; 3C).

Additionally, in the holotype skull, we cannot confirm the suture drawn by Rieppel (2001b, fig. 26B) within the postorbital sensu Schubert-Klempnauer (1975), which separates a more lateral postfrontal from the postorbital. As noted by Rieppel himself, this suture was a reconstruction lacking an observational basis. In this regard, we infer that Schubert-Klempnauer was correct in stating that the postorbitals of *Macroplacus* are large bones—actually larger than in Rieppel's (2001b) more recent interpretation—and form the entire posterior margin of the orbits. Furthermore, the postfrontals meet medially, excluding the frontals from contact with the parietal(s) (Schubert-Klempnauer 1975, fig. 1). In the *Macroplacus* holotype, Rieppel (2001b, p. 53) noted that "the frontoparietal suture remains obscure", a statement that, however, does not contradict our interpretation of the postfrontals intervening between the frontals and the parietals. The lack of frontal-parietal contact, with the postfrontals reaching the midline of the skull (see new character

89), represents a unique character state in *Macroplacus raeticus* among placodonts—possibly with the exception of *Psephochelys polyosteoderma* (Li & Rieppel 2002; Wang et al. 2019b). Notably, in the original description of *Psephochelys* by Li & Rieppel (2002, fig. 1), the postfrontals are depicted as meeting medially (see more detailed discussion under character 89). In MCSNB 13033 (Figs. 2C; 3C), the complete outline of the postfrontals is clearly visible, and their sutural relationships match those observed on the right side of the holotype of *Macroplacus*. In both specimens, the postfrontal is a relatively broad, roughly quadrangular bone that contacts the contralateral postfrontal medially, the frontal anteriorly, the postorbital laterally, and the parietal posteromedially. Anterolaterally, the postfrontal contributes to the dorsal margin of the orbit, which is completed by the frontal (character 66) and, to a lesser extent, the prefrontal. Posteriorly, the postfrontals do not enter the pineal foramen, which is entirely enclosed within the parietal(s), wedging anteriorly between the postfrontals. There are no distinct anterolateral processes of the parietal(s) in both *Macroplacus* holotype and MCSNB 13033 (character 12). According to our interpretation of the frontal, postfrontal, and postorbital in both specimens, the contact between the postorbital and parietal is broad, excluding the postfrontal from the upper temporal fenestra—a condition also observed in *Psephoderma* and other cyamodontoid placodonts (character 16).

Despite the overall similarity in sutural relationships, the postfrontal in MCSNB 13033 (Figs. 2C; 3C) differs from that of the holotype of *Macroplacus* (Fig. 6) in forming a significantly broader contact with the contralateral postfrontal and contributing more extensively to the orbital margin. In MCSNB 13033, the postorbital does not develop a well-defined anteromedial process that would partly exclude the postfrontal from the orbital contour, as observed in the holotype of *Macroplacus*. As a result, the postfrontal-postorbital contact in the *Macroplacus* holotype is convex and sharply angulated at the junction of an anterolateral and a posterolateral margin, whereas in MCSNB 13033, this contact is nearly straight (character 15).

The parietal of MCSNB 13033 is undoubtedly paired, as confirmed by CT imaging (Fig. 4E, H). In the *Macroplacus* holotype, Schubert-Klempnauer (1975) described the parietal as paired, while Rieppel (2000a) considered it unpaired. Based on direct examination of the bone surface in the holotype, we conclude that a suture between paired parietals may be present anterior to the pineal foramen, as illustrated by Schubert-Klempnauer (1975, fig. 1). We could not confirm the presence of a suture posterior to the pineal foramen. However, diagenetic deformation has displaced the left side of the skull roof relative to the right, suggesting a possible original contact between paired but incompletely fused parietals. Under this interpretation, the paired parietals in MCSNB 13033 may reflect its early ontogenetic stage. As described above, in both the *Macroplacus* holotype and MCSNB 13033, the pineal foramen is entirely enclosed within the parietal(s)—a feature shared by nearly all Placodontiformes.

In *Psephoderma* (Fig. S2), the postfrontals are notably smaller than in the *Macroplacus* holotype and MCSNB 13033, and are separated from each other by paired frontals. A distinguishing feature of *Psephoderma* is the placement of the pineal foramen anterior to a distinct step in the skull roof (Neenan & Scheyer 2014); the parietals are fused.

Based on our direct examination of the holotype of *Macroplacus*, and contra Rieppel (2001b), we determined that below the ventral margin of the orbit, the maxilla-jugal contact is posterior to the level of the midpoint of the orbit's longitudinal diameter but anterior to its posterior margin (Fig. 6A) (character 18). The same condition is observed in *Psephoderma* and MCSNB 13033 (Figs. 2A, B; 3A, B). Additionally, in both the *Macroplacus* holotype and MCSNB 13033, the anterior tip of the jugal does not extend anteriorly along the ventral margin of the orbit beyond the midpoint of its longitudinal diameter, whereas in *Psephoderma* it does (character 8).

Regarding the bones forming the temporal arch and their contact pattern in *Macroplacus*, we confirm the interpretations by Schubert-Klempnauer (1975, figs. 3 and 4) and Rieppel (2001b, fig. 26A), contra Pinna (1989, fig. 5) and Nosotti & Pinna (1993, figs. 3 and 4). The latter authors described a large quadratojugal (character 55) in the holotype specimen along with a relatively small squamosal restricted to the uppermost portion of the temporal skull region.

We concur with Schubert-Klempnauer (1975) and Rieppel (2001b) on the presence of a jugal-squamosal contact in the temporal arch of *Macroplacus*. However, in contrast to Rieppel (2001b) and in agreement with Neenan & Scheyer (2014, fig.

2), we do not observe such a contact in *Psephoderma* (character 56).

The temporal fossae of the holotype of *Macroplacus* (Figs. 6; S1) are sufficiently well preserved to permit description of the lateral wall of the braincase. Its general architecture conforms to the typical cyamodontoid condition, characterised by complete obliteration of the cranio-quadrate passage and the presence of a pteroccipital foramen as an alternative route for nerves and blood vessels (Nosotti & Pinna 1996). Rieppel (2001b, fig. 26) did not provide details regarding the precise contours or contact patterns of the bones forming the secondary, ossified lateral wall of the braincase, nor did he comment on the interpretation by Schubert-Klempnauer (1975, fig. 1).

We generally agree with Schubert-Klempnauer's interpretation, except for his assumption that the squamosal forms only the posterior margin of the post-temporal fenestra, being excluded from its dorsal margin by the ventral flange of the parietal. Our observations instead confirm that, as in Cyamodontoidea more broadly, the squamosal in the holotype of *Macroplacus* develops a distinct dorsal process that borders the post-temporal fenestra both caudally and, in part, dorsally. On the right side of the holotype skull, we also observe that the epipterygoid contacts the squamosal—albeit narrowly—above the post-temporal fenestra, thereby excluding the parietal from its margins (Figs. 6A; 7B). This condition is likewise present in *Psephoderma* (Fig. 8C; see discussion under character 24), whereas it remains uncertain in MCSNB 13033. We conclude that in the *Macroplacus* holotype, the post-temporal fenestra is bordered dorsally by the dorsal process of the squamosal and the posterior process of the epipterygoid, anteriorly by the epipterygoid and the prootic, ventrally by the prootic, and posteriorly by the neomorphic otic process of the squamosal. This process, which is relatively short in *Macroplacus*, contacts the prootic (Figs. 6A; 7B, D; 8A). The post-temporal fenestra is notably reduced in *Macroplacus* (character 46, see further discussion below). The prootic foramen is distinct, opening between the epipterygoid and the prootic on the lateral braincase wall and into the occiput. A very similar arrangement is observed in *Psephoderma* specimen MSNM V 471 (Fig. 8C). However, in specimen PIMUZ A/III 1491 (Neenan & Scheyer 2014, fig. 2), the neomorphic otic process of the squamosal appears longer—more similar to that in *Placochelys*—forming the posterior and ventral margins of the post-temporal fenestra and restricting the prootic to its anterior margin. Due to the extensive development of the palatine in the *Macroplacus* holotype, the base of the epipterygoid abuts entirely on that bone. This condition is shared with MCSNB 13033 and possibly with other Placochelyida (see discussion under character 20).

Finally, we emphasise that in the holotype of *Macroplacus*, the pteroccipital foramen is not visible within the temporal fossa (character 30), as its anterolateral margin aligns with the ventral margin of the post-temporal fenestra (Rieppel 2001b). The foramen is visible only in occipital view, indicating that it is positioned posteromedially (the posteromedial margin of the pteroccipital foramen is medial to the dorsal margin of the post-temporal fenestra). We consider this condition to be diagnostic for Placochelyida, in contrast to Cyamodontida. To highlight the difference in the position of the pteroccipital foramen between these clades, we have refined the description of character 30, introducing a new state (Fig. 7; see also "Commented character list and character coding revision" in the "Supplementary contents").

Ventral view (Figs. 6B; S1B)

Interpretations of the bones forming the hard palate and their sutural relationships in the holotype of *Macroplacus* do not differ significantly between Rieppel (2000a, fig. 24B and 2001b, fig. 26C) and Schubert-Klempnauer (1975, fig. 2). However, following Rieppel and contra Schubert-Klempnauer, we confirm—based on direct observation of the holotype specimen—the absence of the ectopterygoid (character 43) in *Macroplacus*. Under this interpretation, the maxilla is excluded from the anterior margin of the subtemporal fossa due to jugal-palatine contact. As stated by Rieppel (2001b), the jugal does not extend posteriorly along the anteromedial margin of the subtemporal fossa (character 9). Rieppel (2001b) also questioned whether the premaxilla contributes to the internal naris in the *Macroplacus* holotype, as depicted by Schubert-Klempnauer (1975, fig. 2A), noting the difficulty in delineating the anterior margin of the vomers. While we acknowledge Rieppel's concerns, our direct examination of the specimen supports Schubert-Klempnauer's interpretation: the premaxilla forms the anterior margin of the internal naris, while the vomers form the medial one.

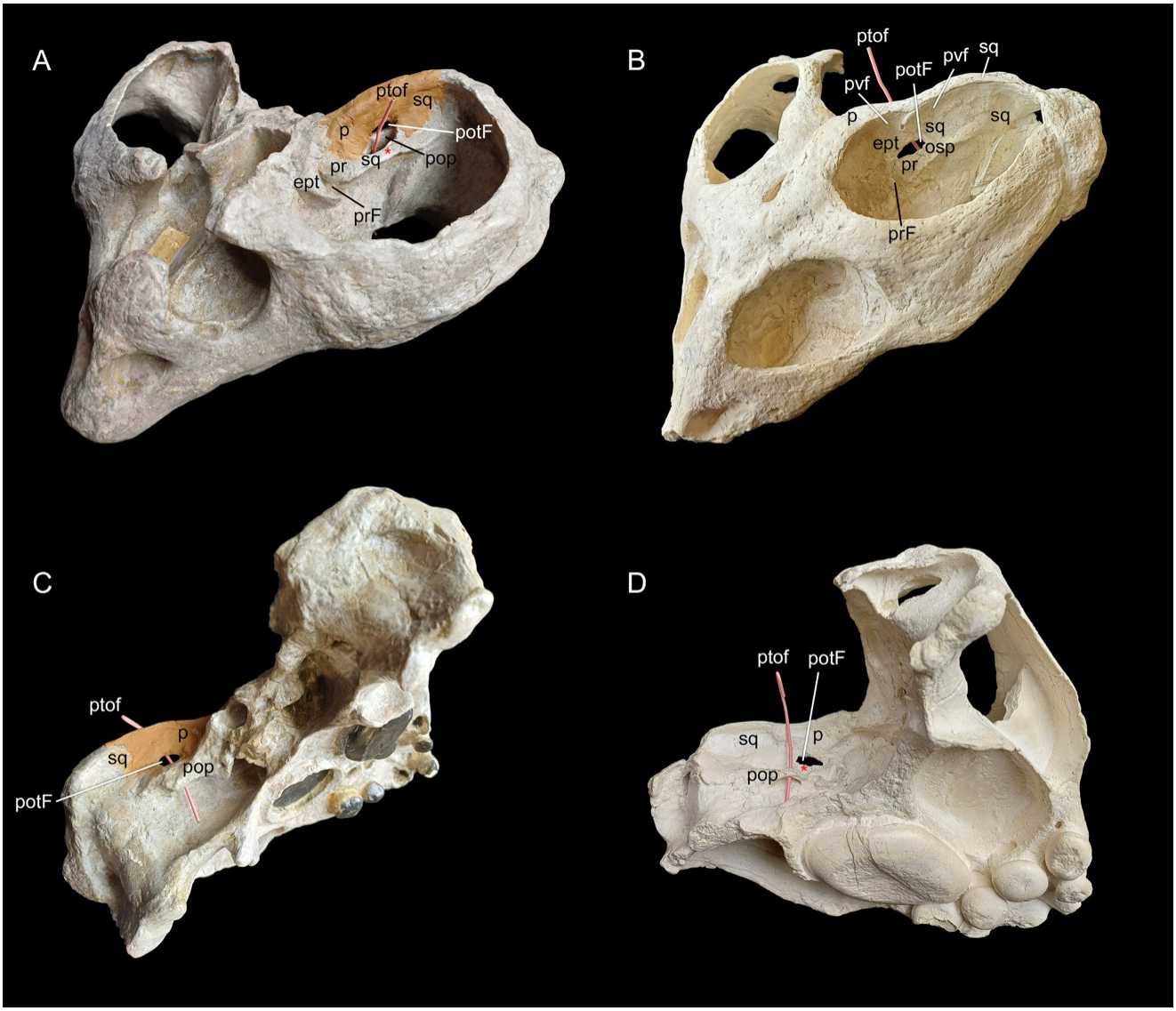

Fig. 7 - Casts of the holotypic skulls of *Cyamodus kuhnschnyderi* (A, C) and *Macroplacus raeticus* (B, D), in anterodorsolateral (A, B) and posteroventrolateral (C, D) views, shown as examples of the character states (1) in Cyamodontida and (2) in Placochelyida, respectively, for character 30. In (A), the anterolateral margin of the pteroccipital foramen lies lateral to the dorsal margin of the post-temporal fenestra, and its posteromedial margin is aligned with it; the foramen is visible within the temporal fossa but not in occipital view. In (B), the anterolateral margin of the pteroccipital foramen is aligned with the dorsal margin of the post-temporal fenestra, and its posteromedial margin lies medial to it; the foramen is visible in occipital view but not within the temporal fossa. A red asterisk marks the squamosal/prootic bridge. The pink stick highlights the position of the pteroccipital foramen relative to the surrounding bones. The missing portion of the temporal bar and the posteromedial margin of the upper temporal fenestra in the *C. kuhnschnyderi* skull were reconstructed in clay. Not to scale. Photos by Simone Maganuco. See "Anatomical abbreviations" section above.

Although the vomers are missing in MCSNB 13033, CT imaging indicates that the elements defining the internal nares exhibit the same pattern of relationships as in the *Macroplacus* holotype (see "Description of the specimen MCSNB 13033" and Fig. 4M). The same configuration was observed in *Psephoderma* by Neenan & Scheyer (2014). According to their study, two small protrusions projecting into the internal nares in *Psephoderma* specimen PIMUZ A/III 1491 represent the posterior remnants of the broken vomers. Similar protrusions in MCSNB 13033 are here interpreted as medial, short processes of the palatines that originally contacted the now-missing vomers (Fig. 4F, I, M).

As described by Rieppel (2001b, p. 49), an anterior process of the maxilla extends into the rostrum, tapering along its lateroventral margin in both the holotype of *Macroplacus* and *Psephoderma*, though it is shorter in the former. CT imaging confirms the same condition in MCSNB 13033 (Fig. 4F).

Neenan et al. (2014) made a significant contribution to our understanding of *Macroplacus* dentition, particularly regarding the tooth replacement pattern, which they investigated in the holotype using micro-computed tomography. Their analysis revealed replacement tooth-plates inside the alveolar spaces (= replacement cavities sensu Rieppel 2001a), all at stage 1 of growth (see Neenan et al. 2014 for the classification of three developmental stages), specifically in tooth positions Lpl2, Lpl1, and Lm2. The corresponding erupted tooth-plates form a crushing functional unit. An erupted Rpl2 tooth-plate is missing and lacks a corresponding replacement tooth-plate, as is the case for Lm1. This suggests that Rpl2 and Lm1 were likely lost due to taphonomic processes. Rpl1 does not have a corresponding replacement tooth-plate, whereas both Rm1 and Rm2 have replacement elements at growth stages 3 and 2, respectively. Based on this pattern, Neenan et al. (2014) determined that *Macroplacus* replaced its tooth-plates in unilateral functional units.

By comparing this pattern with that of most European and Chinese placodont species, Neenan et al. (2014) concluded that unilateral and/or functional unit-based tooth replacement is characteristic of more derived cyamodontoid placodonts. With the exception of *C. kuhnschnyderi*, there is only one replacement element per functional tooth-plate. The posterior, large palatine tooth-plates, along with the corresponding elements in the lower jaws, formed the most effective crushing region of the dentition. Indeed, all highly derived placochelyid specimens examined by Neenan et al. (2014) exhibit at least one replacement tooth-plate in pl2, reflecting the high degree of wear in this tooth position, where the majority of crushing took place. Tooth replacement is minimal anterior to the posterior-most palatine and dentary tooth-plates (Neenan et al. 2014).

MCSNB 13033 has a replacement tooth in Rpl2. However, unlike the *Macroplacus* holotype skull, it also has a second replacement tooth-plate in the contralateral Lpl1. The replacement pattern of the maxillary dentition remains uncertain, as the erupted tooth-plates are not preserved, and the corresponding alveolar spaces are damaged. Given that pl2 is hypertrophied and significantly larger relative to pl1, replacement at the pl2 position was functionally the most important, while replacement in other positions likely had less impact on crushing efficiency and did not require synchronisation with pl2 replacement.

This hypothesis is supported by the observation that none of the highly derived placochelyids analysed by Neenan et al. (2014) exhibit simultaneous replacement of Rpl2 and Lpl2. We conclude that tooth replacement in MCSNB 13033 follows the same pattern described by Neenan et al. (2014) for *Macroplacus*, *Psephoderma*, and cyamodontoid placodonts in general.

Posterior view (Figs. 8A; S1C)

Schubert-Klempnauer (1975, fig. 5) and Rieppel (2001b) provided only a brief description of the occiput in the *Macroplacus* holotype, as it is heavily eroded. However, our direct examination of the specimen allowed us to identify some details of this region. A comparison with MCSNB 13033 is not possible due to its poor preservation (see "Description of the specimen MCSNB 13033").

Contra Schubert-Klempnauer (1975, fig. 5), no tabular bones can be identified in the *Macroplacus* holotype (Rieppel 2001b). The supraoccipital, along with the bones surrounding the foramen magnum—the exoccipitals and basioccipital—are not preserved.

Only remnants of the paroccipital processes are visible, with their distal tips sutured to the squamosals. Unlike in *Psephoderma*, we did not observe a squamosal buttress abutting the distal tip of the paroccipital process (character 47) in the holotype of *Macroplacus* (Fig. 8A). The presence or absence of a posteroventral tubercle at the distal tip of the paroccipital process, which is present in *Psephoderma* (Figs. 8B; S2E)(character 48), cannot be determined in *Macroplacus*.

As noted previously, the post-temporal fenestra in the *Macroplacus* holotype is markedly reduced (character 46), primarily due to the dorsal expansion of the squamosal-prootic bridge dorsal to the pteroccipital foramen. The foramen is visible on the left side of the occiput (Fig. 8A) as a gap between the paroccipital process and the squamosal-prootic bridge. It lies posterior and ventral to the bridge, and is anterolaterally delimited by the posteromedial surface of the bony wall formed by the bridge (Figs. 7B; 8A). In this configuration, the squamosal-prootic bridge forms the ventral margin of the post-temporal fenestra in lateral view (Rieppel 2001b), and the pteroccipital foramen is not visible within the medial wall of the post-temporal fossa. This condition has clear phylogenetic significance, as we recognise it as a

Fig. 8 - The occiput of the holotype of *Macroplacus raeticus* (cast) (A) and of *Psephoderma alpinum* specimen MSNM V 471 (B), and details of the right upper temporal fossa of the latter (C). In (A), the cast was preferred over the fossil because the light colour and shadows make the anatomical details clearer. (A) and (B) are in posterior view, (C) in angled anterodorsal view. Photos by Stefania Nosotti and Simone Maganuco. See "Anatomical abbreviations" section above.

diagnostic feature distinguishing Placochelyida from Cyamodontida (see discussion under character 30 and Fig. 7).

The occiput of *Psephoderma* (Figs. 8B; S2E) exhibits a condition identical to that of the holotype of *Macroplacus* (Figs. 7D; 8A). Despite compression, unequivocal evidence in MSNM V 471 indicates a significant reduction of the post-temporal fenestra, resulting from the dorsal expansion of the squamosal-prootic bridge, which defines the pteroccipital foramen anterolaterally. This foramen is visible only in the occiput and is posteromedially bordered by the paroccipital process of the opisthotic (Figs. 8B; S2E).

In the *Macroplacus* holotype, Schubert-Klempnauer (1975, fig. 5) described triangular projections with broken margins at the anteromedial end of the paroccipital processes, hypothesising that the exoccipitals, opisthotic, and supraoccipital contributed to their formation. We interpret these projections (Fig. 8A) as the otic capsules, originally formed by the prootics, opisthotics, and supraoccipital. The interiors of the otic capsules, now partly filled with sediment, have been exposed. Just anteromedial to these projections, the prootic fenestrae open into the braincase. A completely analogous condition is observed in *Psephoderma* specimen MSNM V 471

(right side of the occiput, Figs. 8B; S2E).

It is noteworthy that a posteromedial position of the pteroccipital foramen relative to the post-temporal fenestra has also been described in *Protenodontosaurus* (Nosotti & Pinna 1999), which, in our phylogenetic analysis, forms the sister group to Cyamodontida + Placochelyida alongside Henodontidae. However, in *Protenodontosaurus* (specimen MFSN 1819 GP; Nosotti & Pinna 1999, figs. 4 and 14), the post-temporal fenestra is notably larger than in *Macroplacus* and *Psephoderma*. In the occiput, the squamosal-prootic bridge does not expand dorsally to form a bony wall dorsal to the pteroccipital foramen, and the anterolateral margin of the foramen aligns with the dorsal margin of the post-temporal fenestra. In *Protenodontosaurus* specimen MFSN 1819 GP (Nosotti & Pinna 1999, figs. 4 and 14), the otic capsules are also exposed in the occiput as large openings in communication with the pteroccipital foramina. However, both are filled with matrix, and the presence of bone inside cannot be ruled out—similar to the condition observed in the otic process of the opisthotic joining the prootic in *Cyamodus kuhnschnyderi* (Nosotti & Pinna 1996, fig. 19). The surrounding bones appear well-preserved, suggesting that the otic capsules in *Protenodontosaurus* may not have been fully ossified (see Nosotti & Pinna 1993, fig. 2 for a comparison of the occiput in *Cyamodus rostratus*, *Protenodontosaurus italicus*, and *Psephoderma alpinum*).

Based on this analysis, we conclude that in the taxa mentioned, state (2) for character 30 (see our extended character description) invariably corresponds to state (1) for character 31, which we have recoded in *Macroplacus* and *Psephoderma*.

Nosotti & Pinna (1993) highlighted the presence of what they termed "accessory connections" between the neurocranium and the hard palate, located posterior to the fused basicranial articulation. These connections contributed to the robust and completely akinetic structure of the placodont skull.

In Cyamodontoidea, Nosotti & Pinna (1993) identified an additional connection between the hard palate and the neurocranium, specifically through the contact between descending processes (ventral flanges) of the opisthotics and the palatal rami of the pterygoids. This condition is clearly visible in the occiput of *Psephoderma* specimen MSNM V 471 (left side), where triangular ventral processes of the opisthotics contact small but well-defined triangular processes arising from the pterygoids (Nosotti & Pinna 1993, fig. 2C; Fig. 8B in this paper).

Two similarly shaped processes emerging from the pterygoids can be seen in the occiput of the *Macroplacus* holotype skull (Fig. 8A), leading us to conclude that the same condition observed in *Psephoderma* is highly probable for *Macroplacus* as well.

Well-developed ventral flanges of the opisthotic closely approaching the posterior margin of the pterygoids were also described by Rieppel (2001b) in the paratype of *Placochelys placodonta* (specimen MB.R. 1765; see discussion in Rieppel 2001b, pp. 17–18, fig. 5B). In other cyamodontoid placodonts, differently developed ventral triangular flanges of the opisthotics can be identified, though they do not reach the quadrate rami of the pterygoids (e.g., Nosotti & Pinna 1993, figs. 2A, B; Nosotti & Pinna 1996, figs. 6 and 18). To address the absence, presence, and potential secondary contact of the opisthotic ventral flange described above, we introduce a new character, character 90, in this paper.

Finally, the floor of the braincase is exposed in the holotype of *Macroplacus*, though its poor preservation prevents a detailed description. However, we can confirm that its internal structure is generally consistent with that described in other cyamodontoid placodonts. The same applies to MCSNB 13033, as far as we have been able to reconstruct this region of the skull through CT slices (see description of the braincase in MCSNB 13033 and Fig. 4A, B, D, E, H).

Placodont phylogenetic analysis (Fig. 9; see also "Supplementary contents")

Methodology for phylogenetic assessment of MCSNB 13033

To assess the phylogenetic affinities of MCSNB 13033, we performed a species-level phylogenetic analysis of Placodontia. To minimise a priori assumptions regarding the presumed monophyly of certain groups or genera, we excluded supraspecific terminal taxa. The taxon set from Wang et al. (2019a) was expanded by incorporating MCSNB 13033 and *Parahenodus atancensis* (de Miguel Chaves et al. 2018b). However, the non-cyamodontoid placodont *Pararcus diepenbroeki* (Klein & Scheyer

2014) from the early Anisian (Lower Muschelkalk) of the Netherlands was excluded due to the absence of cranial material. Similarly, *Glyphoderma robusta* (Hu et al. 2019) was not considered pending more detailed descriptions of the material.

Most characters used in this analysis were sourced from Wang et al. (2019a), whose dataset was based on Neenan et al. (2015), a species-level cranial data matrix for Placodontia that also included two postcranial characters (1 and 63). Neenan et al. (2015), in turn, derived their dataset from Rieppel (2001b) for characters 1–54, Rieppel (2000b; published after Rieppel 2001b) for characters 55–61, and Jiang et al. (2008) for characters 62 and 63. Wang et al. (2019a) further expanded the dataset by incorporating: characters 64–73 from the diapsid analysis in Neenan et al. (2015); characters 74–75 and 76–80, corresponding respectively to characters 55–56 and 58–62 of Rieppel (2000b); and characters 81–88, which pertain to dermal armour. Characters 64-88 for *Psephochelys* and *Parahenodus* were adopted from Wang et al. (2019b). Two new characters characters—89 and 90—are introduced for the first time in this study.

Since the characters included in our expanded dataset were sourced from various authors, each applying different stylistic approaches, we standardised all descriptions according to a consistent editorial format aligned with common cladistic conventions. This was done to ensure clarity, internal consistency, and ease of comparison across taxa. Character statements were also carefully streamlined for conciseness, while maintaining their original informational content and intent.

Character coding was verified through direct examination of specimens by SN, including *Macroplacus*, *Cyamodus hildegardis*, *Cyamodus kuhnschnyderi*, *Cyamodus rostratus*, *Protenodontosaurus*, *Psephoderma*, and *Placodus gigas* (see "Materials and Methods" for specimen details). Several flaws in character definition and coding were identified; therefore, a full list of characters is provided, with all revised character definitions and coding listed and commented upon below each character (see "Commented character list and character coding revision" in the "Supplementary contents").

After revising the character coding, we conducted our own phylogenetic analysis of Placodontia relationships to determine the affinities of MCSNB 13033, which was found to be referable to *Macroplacus*.

The matrix, comprising 19 taxa and 90 characters (see "Supplementary contents"), was subjected to parsimony analysis in PAUP* 4.0a. The analysis yielded a single most parsimonious tree (MPT) with a shortest tree length of 200 steps (CI = 0.5350, RI = 0.6477, RC = 0.3465, HI = 0.4650). The full list of apomorphies supporting each clade is provided in the "Supplementary contents".

Results of phylogenetic analysis (Fig. 9)

Palatodonta is the basalmost representative of the Placodontiformes and the sister taxon to all other Placodontia. The characters supporting Placodontia monophyly are: 10(1) pineal foramen displaced anteriorly on parietal skull table; 58(1) crushing tooth-plates present; 59(1) diastema between symphyseal and posterior dentary teeth present. Placodontia comprises two clades: Placodontoidea and Cyamodontoidea.

As in Analysis 2 of Neenan et al. (2015), but unlike their Analysis 1, Placodontoidea is recovered as a monophyletic group (Fig. 9), with *Placodus inexpectatus* as the sister species to *Placodus gigas*, and *Paraplacodus* as the sister taxon to all other placodonts. Rieppel (2001b) recovered Placodontoidea as monophyletic only after incorporating two postcranial characters into the matrix, though he considered its monophyly weakly supported. In our analysis, Placodontoidea is supported by the following synapomorphies: 37(1) anterior palatine tooth transversely enlarged; 42(1) internal nares confluent; 55(1) quadratojugal absent; 66(1) frontal excluded from dorsal margin of orbit by prefrontal-postfrontal contact; 75(1) hyposphene-hypantrum articulation present; 80(1) lateral gastralia with distinct angulation. ACCTRAN optimisation adds: 63(1) chevron morphology complex as described for *Paraplacodus* by Rieppel (2000b).

Cyamodontoidea is monophyletic (Fig. 9) and is supported by a long list of synapomorphies: 16(2) postfrontal excluded from upper temporal fenestra by broad postorbital–parietal contact; 19(1) dorsal process of epipterygoid broad; 20(1) base of epipterygoid sutured predominantly/entirely to palatine; 26(1) neomorphic otic process of squamosal extends to midpoint of ventral margin of post-temporal fossa; 27(1) palatoquadrate cartilage recess present; 30(1) pteroccipital foramen present, with anterolateral margin lateral to dorsal margin of post-temporal fenestra and posteromedial mar-

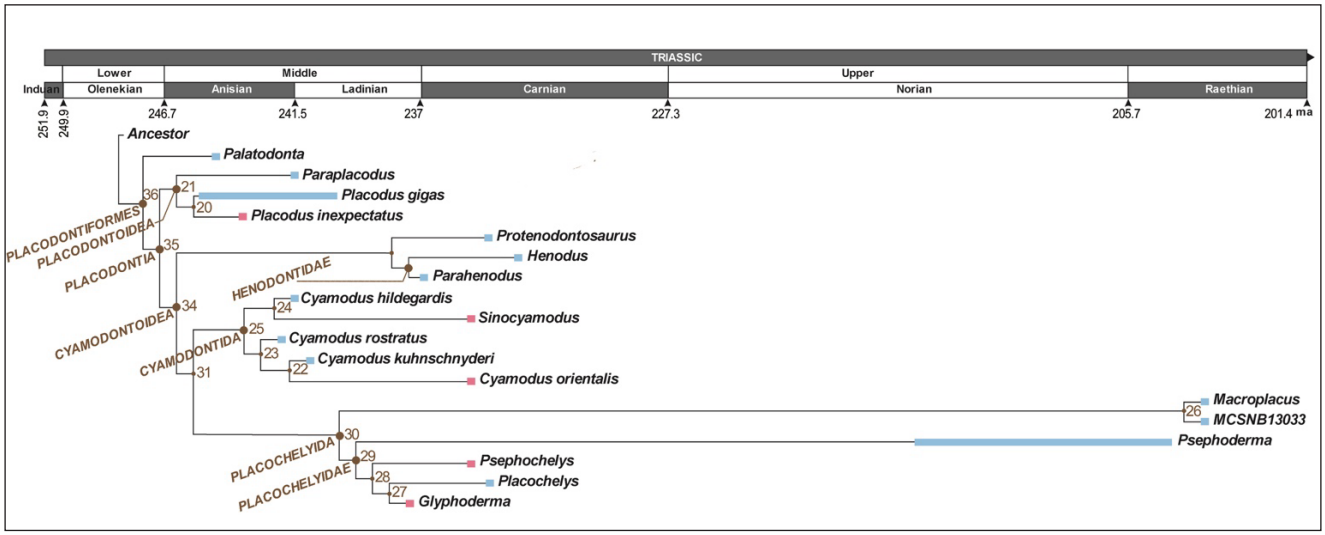

Fig. 9 - Cladogram showing the phylogeny of placodonts according to this study, matching the corresponding distribution of the fossils. Ages of the timeline are based on Cohen et al. (2013), blue/red bars indicate secure fossil occurrences, taxa/strata of the western Tethyan faunas are in light blue, and eastern ones are in light red. The number at nodes are from the Most Parsimonious Tree recovered and are reported into the supplementary information in the character change list, apomorphy list, and reconstructed state for internal nodes in "Phylogenetic data output". Drawing by Angelo Scarcella and Simone Maganuco, redrawn and modified from Wang et al. 2019a.

gin aligned with it, visible within temporal fossa but not in occipital view (1); 35(2) maxilla bearing two teeth; 36(2) palatine bearing two teeth; 43(1) ectopterygoid absent, with palatine-jugal contact; 48(1) posteroventral tubercle ("lateral tubercle" sensu Nosotti & Pinna 1996: p. 19) present; 53(1) retroarticular process short with a sloping surface; 54(2) tubercular osteoderms secondarily fused to underlying bone present along posterior margin of upper temporal fenestra and on lateral surface of posterior temporal arch; 64(1) postorbital region distinctly longer than preorbital region; 74(1) fifteen or fewer dorsal vertebrae; 79(1) intertrochanteric fossa much reduced or absent; 82(1) dorsal carapace present; 90(1) ventral opisthotic flange present not contacting pterygoid; ACCTRAN optimisation adds: 31(1) prootic exposed in posterior view of skull; 38(1) ratio of longitudinal to transverse diameter of posterior palatine tooth exceeds 1.4 in adult; 49(1) exoccipitals meet above occipital condyle (above basioccipital); 51(1) anterior tip of dentary edentulous; 72(1) internal trochanter reduced; 83(1) proximal portion of forelimbs covered under carapace.

It is noteworthy that the highly specialised Henodontidae (*Henodus* and *Parahenodus*), together with *Protenodontosaurus*, form a basal monophyletic group within Cyamodontoidea (Fig. 9). This clade is supported by the following synapomorphies: 4(1) premaxilla ventral surface arched, with rostrum distinctly downturned; 14(1) parietal skull table square with straight lateral margins posteriorly; 35(3) maxilla bearing one tooth. ACCTRAN optimisation adds: 26(2) neomorphic otic process of squamosal extends beyond level of midpoint of ventral margin of post-temporal fossa (in lateral view); 29(1) palatine contacts quadrate along lateral margin of palatoquadrate cartilage recess; 47(1) squamosal buttress present, abutting distal tip of paroccipital process; 85(1) dorsal carapace surface moderately convex with shallow longitudinal groove along midline; 88(1) plastron present. The position of *Protenodontosaurus* is particularly significant, as it might be closer to the basal cyamodontoid bauplan.

The other cyamodontoids clades are Cyamodontida and Placochelyida (Fig. 9). In Neenan et al. (2015*) Henodus* was nested in the former group. Cyamodontida and Placochelyida are united by the following synapomorphies: 24(1) epipterygoid develops a posterior dorsal process contacting squamosal at anterodorsal corner of post-temporal fenestra; 46(1) post-temporal fenestra reduced due to expansion of occipital exposure of parietal, squamosal and prootic; 52(1) coronoid closely approaching ventral margin of mandible; 57(2) coronoid process very high; 67(1) mandibular articulations displaced distinctly behind occipital condyle (1). ACCTRAN optimisation adds: 7(1) anterior end of maxilla expands medially to form most of external naris dermal floor; 18(1) vertical part of maxilla–jugal suture behind level of midpoint of longitudinal diameter

of orbit but in front of its posterior margin; 33(2) anterior premaxillary and dentary teeth bulbous, with anterior transverse ridge.

The characters supporting the monophyly of the Cyamodontida are: 12(1) parietal with distinct anterolateral process embraced by frontal and/or postfrontal; 15(1) posterolateral margin of postfrontal deeply concave and angulated; 65(1) external nares retracted, with longitudinal diameter approaching or exceeding half the longitudinal diameter of orbit. ACCTRAN optimisation adds: 31(0) prootic is not exposed in posterior view of skull; 51(0) anterior tip of dentary with teeth. The Cyamodontida (Fig. 9) includes a clade comprising *Sinocyamodus* and *Cyamodus hildegardis*, united by a single synapomorphy, 35(1) maxilla bearing three teeth. A well-supported clade of the remaining three *Cyamodus* species is defined by the following synapomorphies: 9(1) jugal extends posteriorly along anteromedial margin of subtemporal fossa; 13(1) frontal reaches posteriorly beyond level of anterior margin of upper temporal fossa; 22(1) ratio of basicranial length (snout tip to occipital condyle) to transverse diameter of upper temporal fossa less than 3; 23(1) ratio of longitudinal diameter of upper temporal fossa to longitudinal diameter of orbit equal to/greater than 2 in adult; 39(0) maxilla without anterior process extending into rostrum in ventral view; 45(1) pterygoid ventral flange with double ventral projection. ACCTRAN optimisation adds: 8(1) anterior tip of jugal does not extend anteriorly along ventral margin of orbit beyond midpoint of its longitudinal diameter; 38(0) ratio of longitudinal to transverse diameter of posterior palatine tooth less than 1.4 in adult; 73(2) tarsal ossifications two or fewer. The sister-taxon relationship between *Sinocyamodus xinpuensis* and *Cyamodus hildegardis*, recovered by Neenan et al. (2015), Wang et al. (2019a) and our revised data-set, calls into question the validity of the genus *Sinocyamodus* and suggests that these two taxa might be more appropriately separated at species level. This would allow for a monophyletic genus *Cyamodus*, although, as with all fossil taxa, such taxonomic boundaries remain difficult to establish with precision. Another example of a closely linked European and Chinese species pair is *C. kuhnschnyderi*, which is nested with *C. orientalis*. These sister-taxa share three synapomorphies: 11(1) anterolateral process of frontal reduced; 16(1) postfrontal excluded from upper temporal fossa by narrow postorbital-parietal contact; 28(1) basiorbital furrow present. Kuhn-Schnyder (1959) questioned whether *C. hildergardis* belonged within *Cyamodus*, and Nosotti & Pinna (1996) suggested that the genus may be paraphyletic. It is therefore possible that *Cyamodus hildegardis* and *Sinocyamodus* belong to the same genus, distinct from the other three *Cyamodus* species—though this interpretation remains open to debate and awaits a thorough revision of the relevant fossil material. Wang et al. (2019a) noted that this clade is poorly supported by Bremer and bootstrap values. In line with Kitching et al.'s (1998: 129–131) position, no bootstrap analysis was performed here, as we do not consider such methods informative. Based on the recovered topology, the name Cyamodontidae is not applied to any clade and is treated here as a synonym of Cyamodontida.

The number and diversity of taxa included in our Placochelyida is lower than in Neenan et al. (2015), where Placochelyida also included *Protenodontosaurus*, and in Wang et al. (2019b) which further included *Henodus* and *Parahenodus* (see above). The characters supporting the monophyly of the Placochelyida are: 2(1) ratio of skull total length to skull total height greater than 3; 5(1) premaxilla extends posteriorly along less than half of ventral margin of external naris; 6(1) nasals separated by large posterior (nasal) processes of premaxillae and/or anterior processes of frontals; 17(1) postorbital extends along lateral margin of temporal fossa reaching to level further posterior to midpoint of its longitudinal diameter; 21(1) postorbital develops a medioventral process abutting lateral surface of epipterygoid at posterodorsal margin of foramen interorbitale; 30(2) pteroccipital foramen present, with anterolateral margin aligned with dorsal margin of post-temporal fenestra and posteromedial margin medial to it, visible in occipital view but not within the temporal fossa; 40(1) rostrum ventral surface concave in transverse section. ACCTRAN optimisation adds: 3(1) rostrum relatively narrow and distinctly elongated; 32(1) premaxillary teeth absent; 49(0) exoccipitals do not meet above occipital condyle (above basioccipital); 71(0) carpal ossifications more than three; 76(1) coracoid is a rounded plate of bone; 84(1) carapace osteoderms relatively uniform; 90(2) ventral opisthotic flange contacting pterygoid.

The new specimen MCSNB 13033 is positioned within the Placochelyida as the sister taxon

of the holotype of *Macroplacus raeticus*. Their sister-taxon relationship is supported by the following synapomorphies 8(1) anterior tip of jugal does not extend anteriorly along ventral margin of orbit beyond midpoint of its longitudinal diameter; and 89(1) frontal–parietal contact absent, with postfrontals meeting at skull midline. ACCTRAN optimisation adds: 7(0) anterior end of maxilla does not expand medially to form most of external naris dermal floor; 56(1) jugal–squamosal contact present. Indeed, MCSNB 13033 and the holotype of *Macroplacus raeticus* are here considered to represent the same species—a conclusion based on taxonomic affinities, detailed anatomical comparison, and stratigraphic provenance of the two specimens. In future phylogenetic analyses they should be coded as a single OTU, to increase the number of characters scored for *M. raeticus*.

In this expanded sense, *Macroplacus raeticus*—now understood to include both the holotype and MCSNB 13033—is recovered at the base of the Placochelyida as the sister taxon of the more derived Placochelyidae, contrary to earlier interpretations that placed it less deeply nested within placodont phylogeny (Rieppel 2001b). In Analysis 1 of Neenan et al. (2015), *Macroplacus* was even placed within the Placochelyidae, which is consistent with its considerable morphological similarity to members of that clade. They share 6(1) separated nasals and 3(1) rostrum relatively narrow and distinctly elongated, 41(1) with ventral grooves (as observed in *Placochelys* and *Psephoderma*; still unclear in *Psephochelys*, and unknown in *Glyphoderma*). *Macroplacus* also exhibits a dental morphology that is comparable to, though more extreme than, that of the Placochelyidae; the same dental formula; and a similar tooth replacement pattern (Rieppel 2001a, b; Neenan et al. 2014). *Macroplacus* is the only placodont currently known exclusively from the Rhaetian (latest Triassic), alongside the morphologically similar *Psephoderma*, which occurs in both the Norian and the Rhaetian. This chronostratigraphic and anatomical proximity between the two species lends further support to a close relationship and reinforces the view that the Placochelyidae are the last surviving group of placodonts in the fossil record.

The topology of the Placochelyidae recovered in our analysis places *Psephoderma* as the basalmost member of the group, followed by *Psephochelys*, and finally the sister-taxa *Glyphoderma* and *Placochelys*, which represent the most highly nested taxa. Our results support the revised concept of Placochelyidae introduced by Neenan et al. (2015), comprising *Psephoderma*, *Psephochelys*, *Glyphoderma*, and *Placochelys*. This clade forms a monophyletic group, supported by the following synapomorphies: 41(1) rostrum ventral surface with distinct grooves leading to internal nares; 44(1) ratio of pterygoid palatal ramus length to palatine length greater than 0.3; 47(1) squamosal buttress for distal tip of paroccipital process present. ACCTRAN optimisation adds: 29(1) palatine contacts quadrate along lateral margin of palatoquadrate cartilage recess. The group formed by *Psephochelys* and the sister-taxa *Glyphoderma* and *Placochelys* is supported by the following synapomorphies: 11(1) anterolateral process of frontal reduced; 16(1) postfrontal is excluded from upper temporal fossa by narrow postorbital–parietal contact; 48(0) posteroventral tubercle ("lateral tubercle" in Nosotti & Pinna 1996, p.19) at distal tip of paroccipital process absent; 85(1) dorsal carapace surface moderately convex, with shallow, longitudinal groove along midline. ACCTRAN optimisation adds: 38(0) ratio of longitudinal to transverse diameter of posterior palatine tooth less than 1.4 in adult; 46(0) post-temporal fenestra relatively large; 50(1) basioccipital tuber and ventral opisthotic flange meet ventral to internal carotid passage; 54(1) tubercular osteoderms secondarily fused to underlying bone present along posterior margin of upper temporal fossa only; 69(0) deltopectoral crest well developed; 73(0) tarsal ossifications four or more; 83(0) proximal portion of forelimbs uncovered; 90(1) ventral opisthotic flange present, not contacting pterygoid. Lastly, *Glyphoderma* and *Placochelys* are united by the following synapomorphies: 5(0) premaxilla extends posteriorly along more than half of ventral margin of external naris; 6(0) nasals in contact along midline; 14(1) parietal skull table square with straight lateral margins posteriorly. ACCTRAN optimisation adds: 26(2) neomorphic otic process of squamosal extends beyond level of midpoint of ventral margin of post-temporal fossa (in lateral view); 35(1) maxilla bears three teeth.

Specimen MCSNB 13033 within the Placodontia

Despite the absence of postcranial remains, MCSNB 13033 can be confidently assigned to Placodontia based on the following diagnostic features:

flat, crushing tooth-plates present on palatines and maxillae (character 58), and anteriorly displaced pineal foramen on parietal skull table (character 10). This assignment aligns with the geographic and stratigraphic distribution of placodonts, which are well represented in the Middle and Upper Triassic of Europe, circum-Mediterranean area, and China.

In particular, the skull shape and proportions, the roundish tooth-plates (character 37), and the sutural pattern of the preserved skull bones—including the exclusion of the postfrontal from the upper temporal fossa by a broad postorbital-parietal contact (character 16)—support the assignment of MCSNB 13033 to Cyamodontoidea. This clade also includes the Chinese taxa *Sinocyamodus*, *Cyamodus orientalis*, *Psephochelys* and *Glyphoderma kangi* (Neenan et al. 2015; a second species, *G. robusta*, mentioned above, was more recently described, see Hu et al. 2019). A detailed comparison of MCSNB 13033 with Chinese placodonts, particularly those nesting inside the Placochelyida, is beyond the scope of this paper, as we have not personally examined the material. However, some key points are briefly discussed in the section "Results of phylogenetic analysis".

The dentition of MCSNB 13033, comprising two palatine and two maxillary tooth-plates per side (characters 35 and 36), aligns with the diagnostic pattern of Cyamodontoidea (however, within Cyamodontoidea, the number of maxillary teeth varies from one to five across different taxa, and *Cyamodus rostratus* possesses three palatine tooth-plates per side; Rieppel 2000a and 2001b). The tooth-plate shape and dentition pattern of MCSNB 13033 therefore rule out any affinity with the Placodontoidea. This conclusion is further supported by the absence of an ectopterygoid in MCSNB 13033, which results in direct palatine-jugal contact (character 43). Although the braincase of MCSNB 13033 is poorly preserved, the epipterygoid is interpreted as dorsally broad (character 19) and ventrally abutting only the palatine (character 20), both of which differ from conditions observed in Placodontoidea.

Within Cyamodontoidea, our phylogenetic analysis recovers a monophyletic Henodontidae + *Protenodontosaurus* as the sister group to Cyamodontida + Placochelyida. MCSNB 13033 does not share any diagnostic characters—at least among those identifiable in the specimen—with the former clade, which comprises the highly autapomorphic and incomparable cyamodontid genera *Henodus* and *Parahenodus* (de Miguel Chaves et al. 2018b and 2020). Conversely, MCSNB 13033 shares with Cyamodontida + Placochelyida the vertical part of the maxilla–jugal suture positioned behind the level of the midpoint of the longitudinal diameter of orbit but in front of its posterior margin (character 18).

The three diagnostic characters supporting the monophyly of Cyamodontida (which, in our phylogeny, includes the Chinese genus *Sinocyamodus* and all species of *Cyamodus*) are preserved in MCSNB 13033 but differ in state. Specifically, the new specimen lacks a distinct anterolateral process of the parietal embraced by the frontal and/or postfrontal (character 12) and does not exhibit a deeply concave and angulated lateral margin of the postfrontal (character 15). Regarding the position and shape of the aperturae nasi osseae (character 65), MCSNB 13033 shows an intermediate condition between Cyamodontida and Placochelyidae.

Our analysis recovers Placochelyida as comprising *Macroplacus* and its monophyletic sister clade, Placochelyidae (sensu Neenan et al. 2015), which includes the monospecific genera *Psephoderma*, *Placochelys*, *Psephochelys*, and *Glyphoderma kangi*. As preserved, MCSNB 13033 does not share any of the synapomorphies listed in this paper for Placochelyida (see apomorphy list in "Phylogenetic data output", "Supplementary contents"), except for the concave ventral surface of the rostrum (character 40). However, as previously discussed, we find strong indirect evidence suggesting that the specimen possessed a narrow, elongated, and toothless rostrum—closely resembling that of well-preserved Placochelyida such as *Placochelys* and *Psephoderma*. At the same time, MCSNB 13033 differs from Placochelyidae in lacking distinct grooves on the ventral surface of the rostrum leading up to the internal nares and in having a relatively short palatal ramus (palatal exposure) of the pterygoid (character 44).

Our analysis supports a sister-taxon relationship between MCSNB 13033 and *Macroplacus* within the Placochelyida (see "Results of phylogenetic analysis"). This conclusion results from a partial reinterpretation of SNSB-BSPG 1967 I 324, the holotype skull of *Macroplacus* (see "Re-examination of the holotype of *Macroplacus raeticus*, and comparison with MCSNB 13033 and *Psephoderma alpinum*"). According to the most recent diagnosis of *Macroplacus raeticus* by Rieppel (2000a and 2001b), MCSNB

13033 shares with it the hypertrophied posterior palatine tooth-plates. However, following a close re-examination of the holotype skull, we propose that certain features have been previously misinterpreted. Our findings indicate that SNSB-BSPG 1967 I 324 and MCSNB 13033 exhibit the greatest morphological similarity among placodonts, and their skull proportions, bone arrangement, and dentition strongly support their assignment to the same species, *Macroplacus raeticus*. We consider Schubert-Klempnauer (1975) correct in describing the postfrontals of the *Macroplacus* holotype as reaching the midline of the skull and excluding the frontals from contact with the parietals—a conclusion later rejected by Rieppel (2000a and 2001b). The same pattern is clearly visible in MCSNB 13033, reinforcing the hypothesis that this condition in the holotype of *Macroplacus* is not an artefact of poor preservation or over-preparation, as suggested by other authors (e.g., Rieppel 2001b). The postfrontals contacting each other at the midline and excluding frontal-parietal contact (character 89) is a unique feature within Placodontia, possibly excepting the Chinese placodont *Psephochelys polyosteoderma* (see above).

The substantial size difference between the two specimens (the holotype skull of *Macroplacus* being approximately twice the size of MCSNB 13033) is most parsimoniously explained by their representing different ontogenetic stages of the same taxon, rather than distinct species or a highly dimorphic single species.

As discussed above (see "Geological Setting"), the most probable stratigraphic provenance of MCSNB 13033 is the Zu Limestone (Rhaetian). *Macroplacus raeticus* (also Rhaetian) and *Psephoderma alpinum* (Norian–Rhaetian) represent the latest occurrences not only of Placochelyida but of the entire Placodontia in the fossil record. Within Placochelyidae, *Psephoderma* is the sister taxon to the remaining members of the group, and there is broad agreement that *Psephoderma* and *Macroplacus* share similar, highly specialised morphology, suggesting a close relationship (Neenan et al. 2015 and references therein).

Evidence from taxonomic affinities, anatomical comparisons, provenance, and phylogenetic analysis all support the identification of MCSNB 13033 as *Macroplacus raeticus*, which, in turn, is the sister taxon to Placochelyidae (sensu Neenan et al. 2015). Accordingly, we confirm *Macroplacus raeticus* as a valid genus and species, as stated by Rieppel—contra Pinna (1978, 1990, fig. 1, and 1999, *Psephoderma raeticum* sic!), who hypothesised that it represented a late ontogenetic stage of *Psephoderma alpinum*. Unfortunately, like the *Macroplacus* holotype, MCSNB 13033 lacks postcranial remains, meaning that the diagnosis of *Macroplacus raeticus* remains based solely on cranial material.

Systematic palaeontology

SAUROPTERYGIA Owen, 1860
Placodontiformes Neenan et al., 2013
Placodontia Cope, 1871
Cyamodontoidea Nopcsa, 1923
Placochelyida Romer, 1956

Macroplacus raeticus Schubert-Klempnauer, 1975

Figs. 1-8

Amended diagnosis of *Macroplacus raeticus*: Schubert Klempnauer's diagnosis (1975) of *Macroplacus raeticus* and the most recent one by Rieppel (2000a) (see "Supplementary contents" for more details of the two) were amended by us as follows.

Genus: *Macroplacus* Schubert-Klempnauer, 1975

Type and only known species: *Macroplacus raeticus* Schubert-Klempnauer, 1975.

Holotype: SNSB-BSPG 1967 I 324.

Referred specimen: MCSNB 13033.

Stratum typicum: Kössen Formation, Rhaetian, Upper Triassic.

Locus Typicus: Hinterstein (Sonthofen) in Bad Hindelang, Allgäu, Bavaria, Germany.

Distribution: Rhaetian (Upper Triassic); Bavarian (Germany) and Lombard (Italy) Alps..

Diagnosis: a highly specialised cyamodontoid placochelyid placodont defined by the following combination of characters.

Skull relatively flattened with wide upper temporal fenestrae; powerful crushing dentition with two palatine and two maxillary tooth-plates per side; posterior palatine tooth-plates hypertrophied, covering most of the palatal surface; tightly packed tooth-plates covering the entire extent of the hard palate; premaxillae edentulous at least at their base; rostrum formed by juxtaposed, rod-like premaxillae, ventrally concave with a single median groove, straight in lateral profile, at least basally; an anterior process of the maxilla enters the rostrum; very wide palatine bones forming most of the palatal surface; pterygoid palatal rami drastically shortened anteroposteriorly; ectopterygoid absent; jugal-pala-

tine contact excluding the maxilla from the anterior margin of the subtemporal fossa; jugal not extending posteriorly along the medial margin of the subtemporal fossa; premaxilla forming the anterior margin of the internal naris; nasals not in contact along the midline of the skull; posterior (nasal) processes of the premaxillae enlarged and extending backwards to reach the frontals, thereby separating the nasals from one another; paired frontals; wide postfrontals meeting medially, thus excluding the frontals from contact with the parietals; postfrontals contributing to the dorsal margin of the orbits; paired parietals, probably fused in adult individuals; parietals fully enclosing the pineal foramen; anterolateral processes of the parietals embraced exclusively by the postfrontals; broad postorbital-parietal contact excluding the postfrontal from the upper temporal fenestra; maxilla meeting the jugal ventral to the orbit at a level posterior to the midpoint of the longitudinal diameter of the orbit but in front of its posterior margin; jugal-squamosal contact in the temporal arch; quadratojugal forming two thirds of the ventral margin and ventral portion of the temporal arch; in the temporal fossa, the squamosal forms a distinct dorsal process bordering the post-temporal fenestra posteriorly and partly dorsally; (narrow) squamosal-epipterygoid contact dorsal to the post-temporal fenestra, excluding the parietal from its margin; base of the epipterygoid abutting entirely on the palatine; post-temporal fenestra markedly reduced due to dorsal expansion of the squamosal-prootic bridge, which defines the pteroccipital foramen anterolaterally; pteroccipital foramen located posteromedially (visible only in occipital view) and posteromedially bounded by the paroccipital process of the opisthotic, which extends outward from the occipital surface like a bridge; prootic exposed in posterior view of the skull; no squamosal buttress abutting the distal tip of the paroccipital process; foramen piercing the shaft of the quadrate just above the mandibular condyle; weakly arched gap separating the quadrate-quadratojugal complex from the squamosal in posterior view.

Conclusions

Until now, the cyamodontoid placodont *Macroplacus raeticus* was known only from its holotype skull, SNSB-BSPG 1967 I 324, described by Schubert-Klempnauer in 1975. This study reports a second specimen—MCSNB 13033, a juvenile skull from Italy lacking associated postcranial material—which represents both the first record of the species outside its type locality and the second known worldwide. The Rhaetian age of the Zu Limestone, source of MCSNB 13033, is consistent with the stratigraphic position of the holotype in the Kössen Formation, suggesting faunal correlations between the two units.

The anatomical study of MCSNB 13033, enhanced by CT data, together with a re-examination of the holotype, enables an updated cranial reconstruction and amended diagnosis of *Macroplacus raeticus*. The contact between the postfrontals along the skull midline, excluding the frontals from contacting the parietals, is unique among placodonts and represents a new autapomorphy of *Macroplacus* (character 89). Hypertrophic pl2 is also diagnostic and shared by both the holotype of *Macroplacus* and MCSNB 13033. A detailed redescription of the pteroccipital foramen and its spatial relationships to surrounding structures supports the conclusion that, in *Macroplacus* and other Placochelyida, the spatial configuration in which the anterolateral margin of the pteroccipital foramen aligns with the dorsal margin of the post-temporal fenestra and the posteromedial margin lies medial to it (see character 30) consistently corresponds with prootic exposure in occipital view (see character 31). This correspondence may justify merging the two characters in future analyses. We also provide a more detailed description of the occiput of the holotype of *Macroplacus* and compare it with that of *Psephoderma* (specimen MNSM V471), previously not fully analysed, and introduce character 90 to capture the condition of the ventral flange of the opisthotic—whether absent, present, or in secondary contact.

The description of MCSNB 13033, along with the reassessment of the holotype, substantially expands the placodont dataset—both in quantity and quality—and provides a robust foundation for future phylogenetic and comparative research. This re-evaluation of previously described placodont specimens in light of newly discovered material and improved datasets, demonstrate the potential to refine placodont phylogeny. While the comprehensive revision of character coding across all relevant taxa is beyond the scope of this paper, character defi-

nitions and coding from prior phylogenetic analyses were reviewed and partially revised based on first-hand observations of several European placodonts and informed by recent studies.

A more resolved phylogeny, in turn, is essential for reconstructing palaeobiogeographic and evolutionary scenarios. According to Neenan et al. (2015 and references therein), Placodontiformes likely originated and initially evolved in the Germanic Basin and Alpine Tethys (see Neenan et al. 2013 for further discussion) before dispersal into the eastern Tethys. The earliest record of cyamodontoid placodonts is also from the western Tethys, with *Cyamodus rostratus* and *Cyamodus hildegardis* both known from the Anisian (early Middle Triassic), whereas *Sinocyamodus* does not appear until the Carnian (early Late Triassic). *Protenodontosaurus* and *Henodus* are recorded from the Carnian, as is *Parahenodus* (de Miguel Chaves et al. 2018b; García-Ávila et al. 2021). Based on their phylogenetic position, their common ancestor must have existed by the Middle Triassic, before the divergence of Cyamodontida and Placochelyida. All known Placochelyida, possibly including *Glyphoderma*, are from the Late Triassic. The age of the Zhuganpo Formation, where *Glyphoderma* was discovered, has been debated as either Ladinian or at least partly Carnian (see Wang et al. 2019a and references therein for further discussion; Hu et al. 2019). If *Glyphoderma* is indeed Ladinian, as suggested by recurring phylogenetic results placing it within Placochelyidae (this analysis; Neenan et al. 2015; Wang et al. 2019a), it may indicate that all major placodont clades originated in the Middle Triassic. This time interval, marked by rapid sea-level rise (Wang et al. 2019a and references therein), could have facilitated their diversification and may suggest an eastern (Chinese) origin for Placochelyidae.

To enhance the accuracy of future phylogenetic analyses on placodonts, we recommend incorporating our revised character definitions, rescored character states and a broader revision of character descriptions and scoring across all relevant taxa, particularly those not included in the present study. We also endorse Wang et al. (2019a)'s view that the palaeontological community requires new data on both eastern and western species, as well as additional collections from faunas located between the eastern and western margins of the Tethys, to reconstruct a more reliable biogeographic scenario, dispersal routes, and migration processes, which presently remain unclear and can only be tentatively hypothesised.

Data Availability Statement

The data supporting the results of this research are available upon request. Interested researchers may contact the corresponding Author to obtain access.

Aknowledgements: We warmly thank Anna Paganoni (MCSNB) for the invitation to study the specimen and for granting access to the Palaeontological Collections of Museo Civico di Scienze Naturali, Bergamo; Cristina Longhi (Soprintendenza ABAP BG-BS) for authorisation to study the specimen; Marco Valle and Annalisa Aiello (MCSNB) for their constant support and collaboration throughout the research; Pio Carlo Brizzi who discovered the specimen and promptly delivered it to the Museo Civico di Scienze Naturali, Bergamo; Matteo Malzanni (MCSNB) for assistance during fieldwork; Franco Valoti (photographer) for the photographs of the specimen; Ilaria Paola Crippa (Siemens Milano), Giovanni Longhi (Siemens Milano), Manuel Cecchini (Siemens Milano), and Giovanni Terribile (Fondazione IRCCS Ca' Granda Ospedale Maggiore Policlinico, Milano) for production and post-processing of CT Imaging; Pietro Biondetti (Direttore Radiologia e Area Diagnostica per Immagini Fondazione IRCCS Ca' Granda Ospedale Maggiore Policlinico, Milano) for granting access to the CT Scanner; Oliver Rauhut (SNSB-BSPG) for providing access to the holotype of *Macroplacus raeticus*; Fabrizio Berra (Dipartimento Scienze della Terra Università degli Studi di Milano), Lucia Angiolini (Dipartimento Scienze della Terra Università degli Studi di Milano) and Sergio Chiesa (CNR Consiglio Nazionale delle Ricerche) for valuable discussion, comments and suggestions; Federico Fanti (Alma Mater Studiorum - Università di Bologna) and Matteo Fabbri (University of Johns Hopkins University School of Medicine, Baltimore) for helpful discussions; Marco Auditore for the drawings in Figs. 3, 5-6; Massimo Demma for additional post-processing of CT imaging; Angelo Scarcella for Fig. 9; and Larry Witmer (Ohio University, Athens) for comments on the terminology used here for the three anatomical planes. We are deeply grateful to the anonymous reviewers for their constructive criticism and suggestions, which greatly improved the earlier draft of this paper.

References

Berra F. (2012) - Sea-level fall, carbonate production, rainy days: How do they relate? Insight from Triassic carbonate platforms (Western Tethys, Southern Alps, Italy). *Geology*, 40: 271-274. DOI: 10.1130/G32803.1

Berra F., Jadoul F. & Anelli A. (2010) - Environmental control on the end of the Dolomia Principale/Hauptdolomit depositional system in the central Alps: Coupling sea-level and climate changes. *Palaeogeography, Palaeoclimatology, Palaeoecology,* 290: 138-150. DOI:10.1016/j.palaeo.2009.06.037

Berra F. & Cirilli S. (1997) - Palaeoenvironmental interpretation of the Late Triassic Fraele Formation (Ortles Nappe, Austroalpine Domain, Lombardy). *Rivista Italiana di Paleontologia e Stratigrafia*, 103(1): 53-70.

Boni A. (1946) - Sopra un placodonte Retico del M. Albenza. *Bollettino della Società Geologica Italiana*, 65: 47-48.

Boni A. (1948) - *Placochelys malanchinii* nuova forma di placodonte del Retico lombardo. *Palaentographica Italica*,

43(n.s.13): 1-12.

Bryant H.N. & Russell A.P. (1992) - The role of phylogenetic analysis in the inference of unpreserved attributes of extinct taxa. *Philosophical transaction of the Royal Society of London, Series B,* 337: 405-418.

Buffetaut E. & Novak M. (2008) - A cyamodontid placodont (Reptilia: Sauropterygia) from the Triassic of Slovenia. *Palaeontology*, 51(6): 1301-1306.

Cohen, K.M., Finney, S.C., Gibbard, P.L. & Fan, J.-X. (2013; updated) - The ICS International Chronostratigraphic Chart. Episodes 36: 199-204.

Cope E.D. (1871) - The systematic arrangement of the Reptilia. *Proceedings of the American Association for the Advancement of Science*, 19: 226-247.

Dahdul W.M., Cui H., Mabee P.M., Mungall C.J., Osumi-Sutherland D., Walls R.L. & Haendel M.A. (2014) - Nose to tail, roots to shoots: spatial descriptors for phenotypic diversity in the Biological Spatial Ontology. *Journal of Biomedical Semantics*, 5: 34.

García-Ávila M., De la Horra R., Miguel Chaves C. de, Juncal M.A., Pérez-García A., Ortega F. & Diez J.B. (2021) - Palynological and sedimentological implications of the sauropterygian Upper Triassic site of El Atance (Central Iberian Peninsula). *Review of Palaeobotany and Palynology*, 295: 1-15. DOI:10.1016/j.revpalbo.2021.104541.

Galli M.T., Jadoul F., Bernasconi S.M., Cirilli S. & Weissert H. (2007) - Stratigraphy and palaeoenvironmental analysis of the Triassic-Jurassic transition in the western Southern Alps (Northern Italy). *Palaeogeography, Palaeoclimatology, Palaeoecology,* 244: (2007) 52-70.

Gere K., Nagy A.L., Scheyer T.M., Werneburg I. & Ősi A. (2024) - Complex dental wear analysis reveals dietary shift in Triassic placodonts (Sauropsida, Sauropterygia). *Swiss Journal of Palaeontology*, 143 (4): 1-23. DOI: 10.1186/s13358-024-00304-x

Gnaccolini M. (1965) - Il Calcare di Zu e l'Argillite di Riva di Solto: due formazioni del Retico Lombardo. *Rivista Italiana di Paleontologia e Stratigrafia*, 74(4): 1099-1121.

Gnaccolini M. (1968) - Calcare di Zu. Studi illustrativi della Carta Geologica d'Italia, Formazioni Geologiche, 1: 97-103.

Golebiowski R. (1990) - The alpine Kössen Formation, a key for European topmost Triassic correlations. *Albertiana*, 8: 25-35.

Hu J., Jiang T. & Li Z. (2019) - A new species of *Glyphoderma* (Reptilia: Placodontia) of Middle Triassic from Fuyuan County, Yunnan Province, China. *Journal of Geology*, 43(4): 595-598.

ISPRA (2012) - Carta Geologica d'Italia 1:50.000, Foglio 077, CLUSONE.

Jadoul F., Masetti D., Cirilli S., Berra F., Claps M. & Frisa S. (1994) - Norian-Rhaetian stratigraphy and palaeogeographic evolution of the Lombardy Basin (Bergamasque Alps). In Caramonte G. & Torelli R. (Eds) - Guide book of excursions: 5-38. 15th IAS Regional Meeting, April 1994, Ischia, Italy.

Jadoul F., Galli M.T., Calabrese L. & Gnaccolini M. (2005) - Stratigraphy of Rhaetian to lower Sinemurian carbonate platforms in Western Lombardy (Southern Alps, Italy): paleogeographic implications. *Rivista Italiana di Paleontologia e Stratigrafia*, 111(2): 285-303.

Jadoul F. & Berra F. (2012) - Note illustrative della Carta Geologica d'Italia alla scala 1:50.000, foglio 077 Clusone. APAT - Dipartimento Difesa del Suolo - Servizio Geologico d'Italia.

Jiang D.Y., Motani R., Hao W.C., Rieppel O., Sun Y.L., Schmitz L. & Sun Z.Y. (2008) - First record of Placodontoidea (Reptilia, Sauropterygia, Placodontia) from the eastern Tethys. *Journal of Vertebrate Paleontology*, 28: 904-908.

Kitching I.J., Forey P.L., Humphries C.J., & Williams D.M. (1998) - Cladistics. Second Edition. The Theory and Practice of Parsimony Analysis. Oxford University Press: 1-228.

Klein N. & Scheyer T.M. (2014) - A new placodont sauropterygian from the Middle Triassic of the Netherlands. *Acta Palaeontologica Polonica*, 59(4): 887-902. DOI: 10.4202/app.2012.0147

Kuhn-Schnyder E. (1959) - Über das Gebiß von *Cyamodus*. *Vierteljahrsschrift der Naturforschenden Gesellschaft in Zürich*, 104: 174-188.

Li C. (2000) - Placodont (Reptilia: Placodontia) from Upper Triassic of Guizhou, southwest China. *Vertebrata PalAsiatica*, 38: 316-317.

Li C. & Rieppel O. (2002) - A new cyamodontoid placodont from Triassic of Guizhou, China. *Chinese Science Bulletin*, 47(5): 403-407.

Maisch M.W. (2020) - The evolution of the temporal region of placodonts (Diapsida: Placodontia) - a problematic issue of cranial osteology in fossil marine reptiles. *Palaeodiversity,* 13(1): 57-68. DOI: 10.18476/pale.v13.a6

Mazin J-M. (1989) - La denture et la région palatine des Placodontia (Reptilia, Trias). Implications phylogénétiques. *Geobios*, 22(6): 725-734.

Mazin J-M. & Pinna G. (1993) - Palaeoecology of the armoured placodonts. *Paleontologia Lombarda* N.S., II: 83-91.

Meyer H. von (1858a) - *Psephoderma alpinum* aus dem Dachstein-Kalke der Alpen. *Palaeontographica*, 6: 246-252.

Meyer H. von (1858b) - *Psephoderma alpinum* aus dem Dachstein-Kalke der Alpen. *Neues Jahrbuch für Mineralogie, Geognosie, Geologie und Petrefaktenkunde*: 646-650.

Miguel Chaves C. de, Scheyer T.M., Ortega F. & Perez-García A. (2018a) - The placodonts (Sauropterygia) from the Middle Triassic of Canales de Molina (Central Spain), and an update on the knowledge about this clade in the Iberian record. *Historical Biology*, 32(1): 34-48. DOI: 10.1080/08912963.2018.1462805

Miguel Chaves C. de, Ortega F. & Perez-García A. (2018b) - A new placodont from the Upper Triassic of Spain provides new insights on the acquisition of the specialized skull of Henodontidae. *Papers in Palaeontology*, 4: 567-576.

Miguel Chaves C. de, Serrano A., Ortega F. & Perez-García A. (2020) - Braincase and endocranium of the Placodont *Parahenodus atancensis* de Miguel Chaves, Ortega & Pérez-García, 2018, a representative of the highly specialized clade Henodontidae. *Comptes Rendus Palevol*, 19(10): 173-186. DOI: 10.5852/cr-palevol2020v19a10

Motani R. (2009) - The evolution of marine reptiles. *Evolution: Education and Outreach*, 2: 224-235. DOI: 10.1007/s12052-009-0139-y

Neenan J.M. & Scheyer T.M. (2014) - New specimen of *Psephoderma alpinum* (Sauropterygia, Placodontia) from the Late Triassic of Schesaplana Mountain, Graubünden, Switzerland. *Swiss Journal of Geosciences*, 107(2-3): 349-357. DOI: 10.1007/s00015-014-0173-9

Neenan, J.M., Klein, N. & Scheyer T.M. (2013) - European origin of placodont marine reptiles and the evolution of crushing dentition in Placodontia. *Nature Communica-*

tions, 4(1621): 1-7. DOI: 10.1038/ncomms2633
Neenan J.M., Li C., Rieppel O., Bernardini F., Tuniz C., Muscio G. & Scheyer T.M. (2014) - Unique method of tooth replacement in durophagous placodont marine reptiles, with new data on the dentition of Chinese taxa. *Journal of Anatomy*, 224(5): 603-613. DOI: 10.1111/joa.12162
Neenan J.M., Li C., Rieppel O. & Scheyer T.M. (2015) - The cranial anatomy of Chinese placodonts and the phylogeny of Placodontia (Diapsida: Sauropterygia). *Zoological Journal of the Linnean Society*, 175: 415-428.
Nopcsa F. von (1923) - Die Familien der Reptilien. In: Soergel W. (Ed) - Fortschritte der Geologie und Palaeontologie. Vol. 2. Borntraeger, Berlin: 1-210.
Nosotti S. & Pinna G. (1989) - Storia delle ricerche e degli studi sui rettili placodonti. Parte prima 1830-1902. *Memorie della Società Italiana di Scienze Naturali e del Museo Civico di Storia Naturale di Milano*, XXIV (2): 31-86.
Nosotti S. & Pinna G. (1993) - New data on placodont skull anatomy. In Mazin, J.-M., and G. Pinna (Eds) - Evolution, ecology and biogeography of the Triassic reptiles. *Paleontologia Lombarda*, N.S., 2: 109-130.
Nosotti S. & Pinna G. (1996) - Osteology of the skull of *Cyamodus kuhnschnyderi* Nosotti and Pinna 1993 (Reptilia, Placodontia). *Paleontologia Lombarda,* N.S., 6: 1-42.
Nosotti S. & Pinna G. (1999) - Skull anatomy of *Protenodontosaurus italicus* Pinna 1990 (Reptilia, Placodontia). *Paleontologia Lombarda* N.S., 11: 1-17.
Nosotti S. & Rieppel O. (2002) - The braincase of *Placodus* Agassiz, 1833 (Reptilia, Placodontia). *Memorie della Società Italiana di Scienze Naturali e del Museo Civico di Storia Naturale di Milano*, 31: 3-18.
Owen R. (1860) - Palaeontology or a systematic summary of extinct animals and their geological relations. Adam & Charles Black, Edinburgh: 1-420.
Pinna G. (1976a) - Osteologia del cranio del rettile placodonte *Placochelyanus stoppanii* (Osswald, 1930) basata su un nuovo esemplare del Retico lombardo. *Atti della Società Italiana di Scienze Naturali e del Museo Civico di Storia Naturale di Milano*, 117(1-2): 3-45.
Pinna G. (1976b) - *Placochelys zitteli*, *Placochelys stoppanii*, *Placochelyanus malanchinii*: un caso di sinonimia fra i rettili placodonti retici della famiglia Placochelyidae. *Bollettino della Società Paleontologica Italiana*, 15(1): 107-110.
Pinna G. (1978) - Descrizione di un nuovo esemplare di *Placochelyidae* del Retico lombardo (*Psephoderma alpinum* Meyer, 1858) e discussione sulla sinonimia *Psephoderma-Placochelyanus* (Reptilia Placodontia). *Atti della Società Italiana di Scienze Naturali e del Museo Civico di Storia Naturale di Milano*, 119(3-4): 341-352.
Pinna G. (1979) - Il cranio di un giovane placochelide (*Psephoderma alpinum* Meyer, 1858) del Norico di Endenna (Bergamo). *Atti della Società Italiana di Scienze Naturali e del Museo Civico di Storia Naturale di Milano*, 120(3-4): 195-202.
Pinna G. (1980a) - Ritrovamento di una corazza di Placochelide nel Norico superiore di Endenna (Bergamo). *Atti della Società Italiana di Scienze Naturali e del Museo Civico di Storia Naturale di Milano*, 121(4): 307-315.
Pinna G. (1980b) - *Psephoderma alpinum* Meyer, 1858: rettile placodonte del Retico europeo. Volume Sergio Venzo, Università di Parma: 149-157.
Pinna G. (1989) - Sulla regione temporo-jugale dei rettili placodonti e sulle relazioni fra placodonti e ittiotterigi. *Atti della Società Italiana di Scienze Naturali e del Museo Civico di Storia Naturale di Milano*, 130: 149-158.
Pinna G. (1990) - Notes on stratigraphy and geographic distribution of placodonts. *Atti della Società Italiana di Scienze Naturali e del Museo Civico di Storia Naturale di Milano*, 131: 145-156.
Pinna G. (1992) - *Cyamodus hildegardis* Peyer, 1931 (Reptilia, Placodontia). *Memorie della Società Italiana di Scienze Naturali e del Museo Civico di Storia Naturale di Milano*, XXVI(I): 1-21.
Pinna G. (1999) - Fossilium Catalogus. I: Animalia. Placodontia (Reptilia Triadica). In: Westphal F. (Ed) - Pars 136: 1-75. Backhuys Publishers, Leiden.
Pinna G. & Nosotti S. (1989) - Anatomia, morfologia funzionale e paleoecologia del rettile placodonte *Psephoderma alpinum* Meyer, 1858. *Memorie della Società Italiana di Scienze Naturali e del Museo Civico di Storia Naturale di Milano*, 25: 17-50.
Renesto S. & Tintori A. (1995) - Functional morphology and mode of life of the Late Triassic placodont *Psephoderma alpinum* Meyer from the Calcare di Zorzino (Lombardy, N Italy). *Rivista Italiana di Paleontologia e Stratigrafia*, 101(1): 37-48.
Rieppel O. (1997) - Part II: Sauropterygia, Introduction. In: Callaway J.M. & Nicholls E.L. (Eds) - Ancient Marine Reptiles: 107-119. Academic Press, San Diego.
Rieppel O. (1999) - Phylogeny and palaeobiogeography of Triassic Sauropterygia: problems solved and unresolved. *Palaeogeography*, *Palaeoclimatology*, *Palaeoecology*, 153: 1-15.
Rieppel O. (2000a) - Sauropterygia I - Placodontia, Pachypleurosauria, Nothosauroidea, Pistosauroidea. In: Wellnhofer P. (Ed). Handbuch der Paläoherpetologie, Teil 12A: 1-134. Verlag Dr. Friedrich Pfeil, München.
Rieppel O. (2000b) - *Paraplacodus* and the phylogeny of the Placodontia (Reptilia: Sauropterygia). *Zoological Journal of the Linnean Society*, 130: 635-659.
Rieppel O. (2001a) - Tooth implantation and replacement in Sauropterygia. *Paläontologische Zeitschrift*, 75(2): 207-217.
Rieppel O. (2001b) - The Cranial Anatomy of *Placochelys placodonta* Jaekel, 1902, and a review of the Cyamodontoidea (Reptilia, Placodonta). *Fieldiana N.S.*, 45: 1-104.
Rieppel O. (2002a) - Feeding mechanics in Triassic stem-group sauropterygians: the anatomy of a successful invasion of Mesozoic seas. *Zoological Journal of the Linnean Society*, 135: 33-63.
Rieppel O. (2002b) - Dermal armor of the cyamodontoid placodonts (Reptilia, Sauropterygia*). Fieldiana N.S.*, 46: 1-41.
Rieppel O. & Hagdorn H. (1999) - A skull of *Cyamodus kuhnschnyderi* Nosotti & Pinna 1993, from the Muschelkalk of Wasselonne (Alsace, France). *Paläontologische Zeitschrift*, 73(3/4): 377-383.
Rieppel O. & Nosotti S. (2001) - A skull of *Cyamodus* (Sauropterygia, Placodontia) from the Triassic of Fusea, Province of Udine, Northeastern Italy. *Atti della Società Italiana di Scienze Naturali e del Museo Civico di Storia Naturale di Milano*, 142: 173-183.
Rieppel O. & Zanon R.T. (1997) - The interrelationships of Placodontia. *Historical Biology*, 12: 211-227.
Rieppel O., Mazin J-M. & Tchernov E. (1999) - Sauropterygia from the Middle Triassic of Makhtesh Ramon, Negev, Israel. *Fieldiana N.S.*, 40: 1-85.
Romer A.S. (1956) - The osteology of the Reptiles. The University of Chicago Press: 1-772.
Schubert-Klempnauer H. (1975) - *Macroplacus raeticus* n.g., n.sp. - ein neuer Placodontier aus dem Rät der Bayerischen

Alpen. *Mitteilungen der Bayerischen Staatssamlung für Paläontologie und historische Geologie*, 15: 33-55.

Storrs G.W. (1994) - Fossil vertebrate faunas from the British Rhaetian (latest Triassic). *Zoological Journal of the Linnean Society*, 112: 217-259.

Wang L., Li J., Wang X., Li C., Wu T. & Liu J. (2010) - Biostratigraphy of Triassic marine reptiles in southwest Guizhou and its adjacent area. *Acta Geologica Sinica*, 75(4): 349-353. DOI: 10.1111/j.1755-6724.2001.tb00052.x

Wang W., Li C., Scheyer T. M. & Zhao L. (2019a) - A new species of *Cyamodus* (Placodontia, Sauropterygia) from the early Late Triassic of south-west China. *Journal of Systematic Palaeontology*, 17: 1457-1476.

Wang W., Ma F. & Li C. (2019b) - First subadult specimen of *Psephochelys polyosteoderma* (Sauropterygia, Placodontia) implies turtle-like fusion pattern of the carapace. *Papers in Palaeontology*, 2019: 1-14.

Wang W., Li C. & Wu X.-C. (2019c) - An adult specimen of *Sinocyamodus xinpuensis* (Sauropterygia: Placodontia) from Guanling, Guizhou, China. *Zoological Journal of the Linnean Society*, 185(3): 910-924. DOI:10.1093/zoolinnean/zly080/5236993

Xing L., Klein H., Lockley M.G., Wu X-C., Benton M.J., Zeng R. & Romilio A. (2020) - Footprints of marine reptiles from the Middle Triassic (Anisian-Ladinian) Guanling Formation of Guizhou Province, southwestern China: The earliest evidence of synchronous style of swimming. *Palaeogeography*, *Palaeoclimatology*, *Palaeoecology*, 558: 1-20. DOI: 10.1016/j.palaeo.2020.109943

Zhao L., Li C., Liu J. & He T. (2008) - A new armored placodont from the Middle Triassic of Yunnan Province, southwestern China. *Vertebrata PalAsiatica*, 46: 171-177.

Zou X. D., Balini M., Jiang D.Y., Tintori A., Sun Z.Y. & Sun Y.L. (2015) - Ammonoids from the Zhuganpo Member of the Falang Formation at Nimaigu and their relevance for dating the Xingyi fossil-Lagerstätte (late Ladinian, Guizhou, China), *Rivista Italiana di Paleontologia e Stratigrafia*, 121, 135-161. DOI: 10.13130/2039-4942/6511